bioRxiv preprint doi: https://doi.org/10.1101/2020.05.24.111831; this version posted May 24, 2020. The copyright holder for this preprint (which was not certified by peer review) is the author/funder, who has granted bioRxiv a license to display the preprint in perpetuity. It is made available under aCC-BY-NC-ND 4.0 International license.

Protocadherin 7 localizes to the plasma membrane during mitosis and promotes cytokinesis by a palmitoylation-dependent mechanism

Nazlı Ezgi Özkan-Küçük[1,2], Mohammad Haroon Qureshi[1], Berfu Nur Yiğit[1], Altuğ Kamacıoğlu[1], Nima Bavili[3], Alper Kiraz[3,4], Nurhan Özlü[1,2]

[1]Department of Molecular Biology and Genetics, Koç University, Istanbul, Turkey
[2]Koç University Research Center for Translational Medicine (KUTTAM), Istanbul, Turkey
[3]Department of Physics, Koç University, Istanbul, Turkey
[4]Department of Electrical and Electronics Engineering, Koç University, Istanbul, Turkey

ABSTRACT

Successful cell division requires dramatic reorganization of the cell cortex in coordination with actomyosin cytoskeleton organization, membrane trafficking and cell adhesion. Although the contractile actomyosin ring is considered as hallmark of cytokinesis, in some cell types cell adhesion systems have been shown to drive cytokinesis independently from actomyosin function. We previously reported that Protocadherin 7 (PCDH7) localizes to the mitotic cortex which is required for building up the full mitotic rounding pressure. Here, we show that PCDH7 localizes to the mitotic cell cortex and to the cleavage furrow by a palmitoylation-dependent mechanism. At the cleavage furrow, PCDH7 facilitates the activation of myosin II and successful cytokinesis. Strikingly, PCDH7 promotes cytokinesis even when the myosin II contractility and integrin mediated adhesion are blocked. This work describes a palmitoylation-dependent cortical reorganization which promotes cytokinesis under different conditions.

Cytokinesis; Mitosis; Plasma Membrane; Protocadherin; PCDH7; Cleavage furrow; Myosin; Adhesion; Plasticity; BioID

bioRxiv preprint doi: https://doi.org/10.1101/2020.05.24.111831; this version posted May 24, 2020. The copyright holder for this preprint (which was not certified by peer review) is the author/funder, who has granted bioRxiv a license to display the preprint in perpetuity. It is made available under aCC-BY-NC-ND 4.0 International license.

INTRODUCTION

Cell division is central to life driving many vital cellular events such as proliferation, propagation, development and regeneration (Rieder and Khodjakov, 2003). The main components of cell division are ancient and evolutionarily conserved across eukaryotic cells (Nurse, 1990). Although pathways that orchestrate cell division are conserved from yeast to mammalian cells (Mitchison and Salmon, 2001; Nigg, 2001), very little is known about how these conserved pathways are adjusted to accommodate the needs of cell types with different shapes, sizes, physiology and extracellular environment.

As the cell progresses into mitosis, its morphology and surface undergo dramatic reshaping. Adherent cells transiently round up during mitosis and the daughter cells spread back to regain their interphase morphology during cytokinesis. These morphologic changes are primarily driven by the reorganization of actomyosin cytoskeleton and down-regulation of adhesive systems (Cramer and Mitchison, 1997; Rosenblatt, 2008) and are thought to facilitate the geometric demand of cell division for accurate chromosome segregation (Lancaster et al., 2013; Stewart et al., 2011b).

Successful completion of cytokinesis requires the coordinated action of diverse cellular machineries (Eggert et al., 2006): it requires the regulation of membrane trafficking, cell adhesion, actomyosin cytoskeleton organization, cell contractility as well as core cell division components such as microtubules and chromosomes (Normand and King, 2010). Communication between the midzone to the actin cortex through Rho signaling spatially and temporally regulates the cleavage furrow formation and ensures that the furrow exactly bisects the segregating chromosomes. Furrow ingression and contractile ring assembly, which are driven by actomyosin contraction, are coupled to an increase in plasma membrane surface due to the spatially regulated exocytosis (Eggert et al., 2006).

Although the contractile actomyosin ring is considered as a hallmark of cytokinesis, cell adhesion systems have also been shown to drive cytokinesis independently from actomyosin contractility in some cell types. This myosin II-independent, but adhesion-dependent model of cytokinesis was first described in the slime mold *Dictyostelium discoideum* and later demonstrated in mammalian cells (Kanada et al., 2005; Nagasaki et al., 2009; Uyeda et al., 2000). In Dictyostelium, myosin II heavy chain mutant cells undergo severe cytokinesis defects in suspension, yet, they were viable on substrates (Uyeda et al., 2000). Similarly, when substrate-adherent normal rat kidney (NRK) and HT1080 fibrosarcoma cells were treated with a potent myosin II inhibitor (blebbistatin), furrow ingression still occurred

bioRxiv preprint doi: https://doi.org/10.1101/2020.05.24.111831; this version posted May 24, 2020. The copyright holder for this preprint (which was not certified by peer review) is the author/funder, who has granted bioRxiv a license to display the preprint in perpetuity. It is made available under aCC-BY-NC-ND 4.0 International license.

(Kanada et al., 2005). In retinal pigment epithelium (RPE) cells, following RhoGEF-dependent (Ect2) inhibition of contractile ring assembly, cytokinesis was achieved through integrin-based adhesion. When myosin II was inhibited, only the adherent cells but not the detached cells were able to form cleavage furrow and divide (Dix et al., 2018). This plasticity during the final step of cell division suggests that different cell types in different extracellular environments may require distinct adaptations to successfully complete cytokinesis. Although there are multiple lines of evidence for the role of adhesion system in cytokinesis, the molecular details of these myosin II-independent, but adhesion-dependent pathways remain elusive. Besides, cell cycle-dependent regulation of myosin II-independent cytokinesis and its communication with the cell division machinery are yet to be determined.

Protocadherins (PCDHs) are the largest subgroup of cell surface proteins in the cadherin superfamily (Morishita and Yagi, 2007; Nollet et al., 2000). Although identified as adhesion molecules, the adhesive roles of PCDHs are context dependent. PCDHs can form homophilic and heterophilic interactions that mediate and regulate cell-cell adhesion and downstream signaling during embryonic development as well as in adult tissues (Bradley et al., 1998; Chen et al., 2007; Kahr et al., 2013; Kim et al., 1998; Kuroda et al., 2002; Tai et al., 2010). In our previous study, we compared the cell surface proteome of interphase and mitosis cells and identified PCDH7 as one of the proteins that is enriched on the mitotic plasma membrane and retraction fibers. Knockdown of PCDH7 using siRNAs interfered with the cell rounding and caused a decrease in the mitotic rounding pressure (Ozlu et al., 2015).

Here, we aimed to unravel the underlying mechanism of the cell cycle-dependent localization of PCDH7 and dissect its role in cell division. PCDH7 localized to the plasma membrane at the onset of mitosis and concentrated at the cleavage furrow during cytokinesis. The mitotic cell surface localization of PCDH7 exhibits a dynamic behavior. PCDH7 interacted with adhesion molecules and actomyosin network as well as with palmitoyltransferase. The inhibition of palmitoylation perturbed both mitotic cell surface and cleavage furrow localization of PCDH7. The knockout of PCDH7 caused reduced myosin activity at the cleavage furrow, cytokinesis failure and multinucleation. The deficiency of PCDH7 increased the extent of cytokinesis failure in myosin II-independent, adhesion-dependent RPE1 cells. Moreover, the inhibition of cell adhesion using GRGDSP peptide, which perturbs integrin binding, worsened the phonotype, and caused almost complete failure of cytokinesis. Taken together, our results indicate that the cell division dependent plasma membrane localization of PCDH7 is palmitoylation-dependent. PCDH7 is

bioRxiv preprint doi: https://doi.org/10.1101/2020.05.24.111831; this version posted May 24, 2020. The copyright holder for this preprint (which was not certified by peer review) is the author/funder, who has granted bioRxiv a license to display the preprint in perpetuity. It is made available under aCC-BY-NC-ND 4.0 International license.

important for a successful cytokinesis. We propose PCDH7 as a novel component of the mitotic cortex that facilitates the coordination of myosin II dependent and independent cytokinesis pathways.

RESULTS

PCDH7 localizes to the cleavage furrow during cytokinesis

Our previous study revealed that PCDH7 enriched at the cell surface as the cell progresses into mitosis (Ozlu et al., 2015). To probe the spatiotemporal regulation of PCDH7, we analyzed its subcellular localization throughout the cell cycle. For this, we preferred to use PCDH7-BAC-GFP cell line in which, GFP tagged PCDH7 is expressed under its own promoter using bacterial artificial chromosome (BAC) transgenomics (Poser et al., 2008). Immunostaining of PCDH7-BAC-GFP cells showed that PCDH7 localized to the cell-to-cell contacts during interphase (**Figure 1A**-top panel), enriched at the cell surface and retraction fibers at the onset of mitosis (**Figure 1A**-middle panel) and concentrated at the contractile ring and midbody during cytokinesis (**Figure 1A**-lower panels). We observed a similar cleavage furrow and contractile ring localization of PCDH7 in HeLa S3 cells expressing PCDH7:eGFP (**Figure 1B**, **Video S1**). These results suggest that the localization of PCDH7 is regulated in a cell cycle-dependent manner.

PCDH7 reveals a dynamic behavior at the mitotic cell surface

To address the dynamicity of PCDH7 translocation to the mitotic cell surface by employing Fluorescence Recovery After Photobleaching (FRAP), we compared the mobility of PCDH7:GFP during interphase with mitosis using PCDH7-BAC-GFP cells. The GFP signal within the region of interest (ROI) at the plasma membrane of both mitotic (**Figure 2A**-top panel) and interphase (**Figure 2A**-bottom panel) cells were photobleached using a focused laser beam. The fluorescence recovery within ROI was analyzed (**Figure 2B**) using a double normalization algorithm (Phair et al., 2004) and fixed-sized ROI areas (Kappel, 2004). After photobleaching, a significant difference was not observed between the recovery levels of PCDH7:GFP in cell to cell contacts during interphase (average recovery 46.6%) and at the plasma membrane during mitosis (average recovery 45%), as shown in **Figure 2C**. However, PCDH7:GFP recovered significantly faster at the mitotic cell surface with an average FRAP half time around 62 seconds, when compared to the cell-to-cell contacts in interphase where average FRAP half time was around 109 seconds (**Figure 2D**). We conclude that PCDH7 is much more dynamic and shows a high turnover rate at the mitotic cell surface in comparison to the cell-to-cell contact regions.

bioRxiv preprint doi: https://doi.org/10.1101/2020.05.24.111831; this version posted May 24, 2020. The copyright holder for this preprint (which was not certified by peer review) is the author/funder, who has granted bioRxiv a license to display the preprint in perpetuity. It is made available under aCC-BY-NC-ND 4.0 International license.

Actomyosin network and adhesion molecules are the proximal interaction partners of PCDH7

To address whether the interaction partners of PCDH7 are involved in its cell cycle-dependent translocation, we employed a proteomic approach using the proximity dependent biotinylation (BioID) method (Roux et al., 2012). In this method, the protein of interest is fused to a promiscuous biotin ligase BirA*, which biotinylates proteins in proximity to the bait and then the biotinylated proteins are identified using mass spectrometry. Initial immunofluorescence analysis revealed that the PCDH7:BirA* recombinant protein exhibited the expected localization pattern in both mitosis and interphase cells and specifically biotinylated the vicinity **(Figure 3A)**.

In order to biochemically assess the biotinylation efficiency and specificity, cells were transfected with PCDH7 (PCDH7:BirA*-HA) and control constructs (truncated PCDH7 BioID vector (PCD7Δcyt:BirA*-HA), unrelated BioID vectors (MyrPalm:BirA*-HA) and empty BioID vectors (BirA*-HA and myc-BirA*)). Transfected and untransfected cells were grown either in regular (- Biotin) or biotin supplemented (+ Biotin) media and the biotinylated proteins were affinity purified from whole cell lysates using streptavidin beads. In the absence of biotin, only a basal level of biotinylation was observed for all cell lines (**Figure 3B**-bottom panel). In the presence of biotin, while non-transfected cells showed a basal level of biotinylation, nonspecific biotinylation was observed for the empty BioID vector transfected cells (**Figure 3B**-top left panel). The inputs (I) obtained from PCDH7 BioID, truncated PCDH7 BioID and MyrPalm BioID transfected cells demonstrated different biotinylation patterns as expected. The biotinylated proteins were successfully enriched at the elute fractions (E) of each sample after streptavidin affinity pulldown (**Figure 3B**-top right panel). Next, pulldown elution samples were blotted against PCDH7 and actin antibodies. The full-length PCDH7 was only present in the elute (E) fraction of PCDH7 BioID transfected cells, but not in the truncated PCDH7 BioID transfected cells. PCDH7 was not detected at all in the elute of MyrPalm BioID sample as expected. (**Figure 3C**-top panel). The absence of actin in the elute fractions confirmed the lack of cytosolic contamination (**Figure 3C**-bottom panel). These results supported the efficient and specific biotinylation of PCDH7 BioID.

In order to discover the interphase and mitosis specific interaction partners of PCDH7, the biotinylated proteins that were isolated from PCDH7 BioID transfected mitotic and interphase cells using streptavidin beads were analyzed in LC-MS/MS. Non-transfected, but biotin supplemented cells were used as a control. The significant interactors were

bioRxiv preprint doi: https://doi.org/10.1101/2020.05.24.111831; this version posted May 24, 2020. The copyright holder for this preprint (which was not certified by peer review) is the author/funder, who has granted bioRxiv a license to display the preprint in perpetuity. It is made available under aCC-BY-NC-ND 4.0 International license.

then identified by calculating the spectral count-based fold change between control and PCDH7 BioID cells of 4 biological replicates with a false discovery rate (FDR) of 0.05 (Choi et al., 2015). We identified 78 proteins for mitosis and 129 for interphase cells (**Table S1**), 49 of which were common in both groups. Those proteins were then analyzed using STRING database (Szklarczyk et al., 2019) and clustered according to GO and KEGG pathway enrichments (Raudvere et al., 2019) using StringApp (Cline et al., 2007; Doncheva et al., 2019). Significant clusters include cell adhesion and cadherin binding proteins, actomyosin network related proteins, vesicular proteins and ERM family proteins (**Figure 3D**).

Palmitoylation is required for the mitotic surface localization of PCDH7

Among many interesting candidates, one striking interaction partner of PCDH7 was a palmitoyltransferase (ZDHHC5) that adds the palmityl group to the proteins. Palmitoylation is a reversible post translational modification that is known to affect the hydrophobicity, the membrane domain interactions and the conformation of transmembrane proteins (Blaskovic et al., 2013). Thus, we decided to test the role of palmitoylation on PCDH7's cell cycle-dependent cell surface translocation. For this purpose, we utilized a standard palmitoylation inhibitor, 2-bromopalmitate (2BP) (Webb et al., 2000).

First, we tested the effect of the palmitoylation inhibitor on PCDH7's hydrophobicity using TritonX-114 extraction, which separates proteins into detergent and aqueous phases according to their hydrophobic properties (Bordier, 1981). The inhibition of palmitoylation decreased the proportion of PCDH7 in the detergent phase suggesting a reduction in the hydrophobicity of PCDH7 (**Figure S1**).

To examine the impact of the palmitoylation inhibitor on the subcellular localization of PCDH7 in mitosis and interphase cells, we performed immunostaining and live imaging of a PCDH7-BAC-GFP cell line treated with 2BP. The inhibition of palmitoylation did not show a noticeable effect on the localization of PCDH7 at the cell-to-cell contacts during interphase **(Figure 4A)**. However, it dramatically decreased the surface localization of PCDH7 in mitotic cells and increased the concentration of PCDH7 at the inner part of the cell (**Figure 4B**). Live imaging of PCDH7 also supported these results (**Figure 4C, Video S2).**

Next, we took a biochemical approach to confirm the detected change in mitotic cell surface localization of PCDH7 upon palmitoylation inhibitor treatment. For this, HeLa S3 cells were treated with 2BP or DMSO (control) overnight,

bioRxiv preprint doi: https://doi.org/10.1101/2020.05.24.111831; this version posted May 24, 2020. The copyright holder for this preprint (which was not certified by peer review) is the author/funder, who has granted bioRxiv a license to display the preprint in perpetuity. It is made available under aCC-BY-NC-ND 4.0 International license.

while being synchronized to interphase or mitosis. To assess the surface localization of PCDH7 after the 2BP treatment, the surface exposed proteins were labelled with a non-permeable sulfo-NHS-SS-biotin reagent followed by affinity purification of biotinylated proteins using streptavidin (Ozkan Kucuk et al., 2018). While the 2BP treatment did not affect the PCDH7 level exposed to the surface in interphase cells (**Figure 4D**-left panel), it strikingly decreased the amount of PCDH7 at the mitotic cell surface (**Figure 4D**-right panel).

To further investigate the effect of the palmitoylation inhibitor on the dynamic behavior of PCDH7 at the mitotic cell surface, we again took the FRAP approach and measured the extent of PCDH7:GFP recovery at the plasma membrane after photobleaching, in the absence or presence of 2BP. As expected, the inhibition of palmitoylation did not have a significant effect on the FRAP recovery of PCDH7 at the cell-to-cell contacts during interphase (**Figure 4E**-left). On the other hand, 2BP treatment dramatically increased the FRAP recovery time of PCDH7 at the mitotic plasma membrane (**Figure 4E**-right). Finally, we analyzed the effect of 2BP during cytokinesis. Inhibition of palmitoylation explicitly perturbed the cleavage furrow localization of PCDH7 during cytokinesis (**Figure 4F**-left) and led to a diffused distribution of PCDH7 all over the dividing cell (**Figure 4F**-right). We conclude that palmitoylation is dispensable for a stable cell-to-cell contact localization of PCDH7 during interphase, but essential for the cortical and cleavage furrow localization of PCDH7 during mitosis and cytokinesis, respectively. The progression of mitosis and cytokinesis were not grossly perturbed by 2BP in these experiments, indicating specificity of the drug.

PCDH7 is required for full myosin II activation during cytokinesis in HeLa S3 cells

Our previous investigation of PCDH7 function during cell division was restricted to the development of mitotic rounding pressure and used siRNA-based depletion of PCDH7 (Ozlu et al., 2015). To obtain more rigorous data, we utilized CRISPR-Cas9 genome editing system (Ran et al., 2013) to knockout PCDH7 in HeLa S3 and RPE1 cells. PCDH7 was targeted using four individual guide RNAs (sgRNA). Control cells were treated with non-targeting guide RNA (sgNT) in parallel. The knockout of PCDH7 in isolated colonies were validated by Western blot analysis. One colony was selected for each cell line (sg1 colony2 for HeLaS3 and sg2 colony6 for RPE1) to proceed with the phenotypic characterization (**Figure S2A**). Control cells (sgNT) were used as pooled population.

We first examined the cytokinesis failure in PCDH7 knockout (KO) HeLa S3 cells to assess its role in cell division. While 5.5% of control HeLa S3 cells exhibited multinucleation, this percentage significantly increased up to 12.5%

bioRxiv preprint doi: https://doi.org/10.1101/2020.05.24.111831; this version posted May 24, 2020. The copyright holder for this preprint (which was not certified by peer review) is the author/funder, who has granted bioRxiv a license to display the preprint in perpetuity. It is made available under aCC-BY-NC-ND 4.0 International license.

in PCDH7 KO HeLa S3 cells (**Figure 5A-B**). The expression of PCDH7:GFP in PCDH7 KO (**Figure S2B**) significantly decreased the multinucleation percentage back to the control level (5.5%) cells and so, rescued the phenotype **(Figure 5B)**.

To characterize the defect leading to multinucleation, we performed live imaging of both control and PCDH7 KO cells. Although PCDH7 KO cells were able to round-up and progress into mitosis, they spent significantly longer time in mitosis compared to control cells. This could be rescued by the ectopic expression of PCDH7:GFP (**Figure 5C**). In agreement with the high rate of multinucleation, about 20% of PCDH7 KO cells failed to divide (**Figure 5D**-Bars 1-2). Although the cleavage furrow initially formed in the majority of cases, the failure in the completion of cleavage furrow ingression resulted in the frequent reunion of daughter cells **(Figure 5E, Video S3**). While the expression of PCDH7:GFP in knockout cells successfully rescued this phenotype (**Figure 5D**-Bars 2-4, **Figure S2E, Video S3**), the expression of GFP alone did not (**Figure 5D**-Bars 2-3, **Figure S2D, Video S3**).

Our previous study showed that PCDH7 is required for the development of full mitotic rounding pressure (Ozlu et al., 2015). Rounding pressure is dependent on myosin II activity (Stewart et al., 2011a; Stewart et al., 2011b), and our BioID data also indicated a close relation between PCDH7 and the actomyosin network. To test whether PCDH7 plays a role in the activation of myosin during cleavage furrow constriction, we analyzed the phospho-myosin II (S19) (Matsumura et al., 1998) levels at the cleavage furrow. The phosphorylated myosin, which was significantly enriched at the cleavage furrow in control cells, was significantly reduced in PCDH7 KO cells (**Figure 5F**). The ratio of phospho-myosin II levels at the cleavage furrow to polar cortex was significantly lower in PCDH7 KO cells compared to control cells (**Figure 5G)**. The quantification of phospho-myosin II intensity also showed a lack of accumulation of activated myosin at the cleavage furrow (**Figure 5H**). As the actin levels at the cleavage furrow did not show any difference between PCDH7 KO and control cells **(Figure 5I),** the reduction of phospho-myosin II can not be due to the impaired actin cytoskeleton at the cleavage furrow. Taken together, our data suggest that PCDH7 positively regulates myosin II activity during cytokinesis.

PCDH7 is essential for the adhesion-dependent cytokinesis in RPE1 cells

The cell adhesion machineries were reported to drive cytokinesis independent of the contractile ring in some cell types. For instance, RPE1 cells were recently shown to undergo adhesion-dependent cytokinesis when the myosin II

bioRxiv preprint doi: https://doi.org/10.1101/2020.05.24.111831; this version posted May 24, 2020. The copyright holder for this preprint (which was not certified by peer review) is the author/funder, who has granted bioRxiv a license to display the preprint in perpetuity. It is made available under aCC-BY-NC-ND 4.0 International license.

dependent-cytokinesis is inhibited (Dix et al., 2018). Although we demonstrated that PCDH7 regulates the activity of myosin II in HeLa S3 cells, we wondered whether PCDH7 is also involved in the adhesion-dependent cytokinesis independent of cortical actomyosin contraction. For this, we first knocked out PCDH7 in RPE1 cells using CRISPR/Cas9 mediated gene editing (**Figure S2C**). When we monitored the cell cycle progression of PCDH7 KO RPE1 cells, we did not observe a significant degree of cytokinesis failure (**Figure 6A**-Bars 1-3), in contrast to PCDH7 KO HeLa S3 cells (**Figure 5D**). This might be due to a redundant cytokinesis mechanism that depends on cell adhesion in the absence of myosin II contraction. Indeed, when RPE1 cells were treated with the myosin II inhibitor blebbistatin (Straight et al., 2003), they were still able to divide, though with an increased cytokinesis failure rate (**Figure 6A**-Bars 1-2). This confirms their ability to achieve contractile ring-independent, adhesion-dependent cytokinesis (**VideoS4**).

We next investigated the function of PCDH7 in the adhesion-dependent cytokinesis by treating PCDH7 KO RPE1 cells with blebbistatin. Strikingly, while control cells still divided at high concentrations of blebbistatin due to the adhesion-dependent cytokinesis (**Figure 6C**-left panel), PCDH7 KO RPE1 cells failed to divide, more often under these conditions (**Figure 6C**-right panel). When myosin activity is inhibited, knockout of PCDH7 caused almost two fold more cytokinesis failure (57%) compared to only blebbistatin treated control cells (35%) (**Figure 6A**-Bars 2-4, **VideoS4**) implying the importance of PCDH7 in adhesion-dependent cytokinesis.

Next, to test whether PCDH7 functions in adhesion-dependent cytokinesis via integrin binding, we exploited GRGDSP peptide that was used to interrupt the binding of integrin to the substrate (Gilchrist et al., 2007). The GRGDSP peptide treatment in RPE1 cells had no profound effect on cytokinesis in both control and PCDH7 KO cells when the actomyosin ring is functional (**Figure 6B**-Bars 1-3). However, in the presence of blebbistatin, the GRGDSP peptide treatment significantly increased cytokinesis failure up to 62% (**Figure 6B**-Bar 2), which is higher than the percentage observed in only blebbistatin treated cells (**Figure 6A**-Bar 2). Moreover, the inhibition of cell adhesion and myosin II activity in PCDH7 KO RPE cells showed an additive effect and caused almost complete (98%) cytokinesis failure in these cells (**Figure 6B**-Bar4). These data suggest that the function of PCDH7 gains importance in cytokinesis when cells are deprived of both myosin II contractility and integrin-mediated adhesion.

Next, we examined the effects of additive perturbations described above on the stability of cleavage furrow in RPE1 cytokinesis cells with microscopy. As anillin is a contractile ring component (Field and Alberts, 1995), it was used as

bioRxiv preprint doi: https://doi.org/10.1101/2020.05.24.111831; this version posted May 24, 2020. The copyright holder for this preprint (which was not certified by peer review) is the author/funder, who has granted bioRxiv a license to display the preprint in perpetuity. It is made available under aCC-BY-NC-ND 4.0 International license.

a cleavage furrow marker in this study. The GRGDGSP peptide treatment had no detectable effect on the integrity of the cleavage furrow in neither control nor PCDH7 KO cells (**Figure 6D**-second row). Blebbistatin treatment caused a mild disorganization and broadening of the cleavage furrow in control cells, as expected (**Figure 6D**-third row, left). However, this effect became more apparent in PCDH7 KO cells (**Figure 6D**-third row, right). The combinatorial usage of two inhibitors caused severe disorganization of the cleavage furrow in both control and PCDH7 KO cells (**Figure 6D**-fourth row).

Taken together, PCDH7 is important for the adhesion-dependent cytokinesis in RPE1 cells in the absence of functional myosin II. Inhibiting the integrin binding alone perturbs cytokinesis but does not completely block it. The inhibition of both myosin II and integrins caused a strong cytokinesis block. About 50% of cells were still able to divide, which was completely dependent on PCDH7.

DISCUSSION

This study aimed to understand how PCDH7 becomes enriched on the surface of mitotic cells, and its function in cytokinesis. Our analysis revealed an unprecedent role of palmitoylation in the translocation of PCDH7 to the mitotic cell surface and cleavage furrow. Palmitoylation is a reversible posttranslational modification that plays a key role in controlling protein targeting by increasing the hydrophobicity of a protein (Linder and Deschenes, 2007). Our BioID based proximity interactome identified a palmitoyl transferase ZDHC5, as a significant interactor of PCDH7. Thus, we hypothesized that palmitoylation might facilitate the plasma membrane translocation of PCDH7 during mitosis and used palmitoylation inhibitor 2BP to test this. Indeed, the cell surface and cleavage furrow localization during mitosis and cytokinesis, respectively was dependent on the palmitoylation, whereas the localization to the cell-to-cell contacts during interphase was not affected by the palmitoylation inhibition **(Figure 4)**. This suggests that two different pools via different mechanisms are targeted to the mitotic cell surface and cell-to-cell contact regions. This notion is also supported by the FRAP analysis which reveals that the turnover rate and dynamics of these two pools are different. However, more work is required to determine whether the observed effect is due to palmitoylation of PCDH7 itself or some other mediator factors. Our attempts of mutating potential palmitoylation sites did not cause a prominent effect on the localization of PCDH7. However, this is rather challenging because of the lack of a consensus motif for protein palmitoylation. Beside cysteine, palmitoylation can also occur on serine and lysine residues. In addition, a cumulative effect of palmitoylation on multiple cysteine, and even on serine or lysine (Brownlee and Heald,

bioRxiv preprint doi: https://doi.org/10.1101/2020.05.24.111831; this version posted May 24, 2020. The copyright holder for this preprint (which was not certified by peer review) is the author/funder, who has granted bioRxiv a license to display the preprint in perpetuity. It is made available under aCC-BY-NC-ND 4.0 International license.

2019) residues might be involved, thus mutating individual residues might not be enough to mimic the effect of the inhibitor. Similarly, PCDH1, which shares 46% homology with PCDH7, was also reported to localize to the membrane in a palmitoylation-dependent manner. However, mutating its cysteine that is known to be palmitoylated was not sufficient to mimic the palmitoylation inhibitor's effect either (Fukata and Fukata, 2010; Kahr et al., 2013).

Although many studies have indicated the role of protein palmitoylation in protein trafficking (Linder and Deschenes, 2007) and different intracellular signaling pathways (Resh, 2006), the importance of palmitoylation in the context of cell division has been emerging only recently. Depalmitoylation activity has been shown to be required for the unequal partitioning of the Notch and Wnt signaling during asymmetric cell division (Stypulkowski et al., 2018). Palmitoylation-dependent membrane association of importin α has been shown to affect the mitotic spindle and nuclear scaling during Xenopus embryogenesis (Brownlee and Heald, 2019). In this study, we have demonstrated that the mitotic cortex and cleavage furrow localization of PCDH7 is palmitoylation-dependent. This may be the first representation of palmitoylation in cell division. Future studies will uncover the underlying molecular mechanism and help us to understand the details of palmitoylation specific cortical reorganization during cell division.

What is the function of PCDH7 during cell division? Our earlier study demonstrated that plasma membrane localization of PCDH7 was important for mitotic rounding and building up the full mitotic rounding pressure (Ozlu et al., 2015). In the present study, we have shown that the knockout of PCDH7 caused a significant increase in mitosis duration **(Figure 5C)** as well as cytokinesis failure in HeLa S3 cells **(Figure 5D)**. Even though PCDH7 KO HeLa S3 cells were able to initiate furrowing, they failed to divide and formed multinucleated cells **(Figure 5E)** or died before they could exit cell division. Actomyosin network is important for mitotic rounding and cleavage furrow formation and both processes seem to be affected in the absence of PCDH7. In addition, our BioID data revealed that PCDH7 is in close proximity with the components of the actomyosin ring including myosin light and heavy chains **(Figure 3D)**. Therefore, we hypothesized that PCDH7 might be involved in the regulation of myosin activity. To test this hypothesis, we compared the active myosin levels at the cleavage furrow during cytokinesis. The phosphorylated myosin level at the cleavage furrow was significantly reduced in the absence of PCDH7 (**Figure 5G, H)** compared to the control cells (**Figure 5F**-left**)**. Collectively, these results suggest that PCDH7 is required for the activity of myosin at the cleavage furrow and proper functioning of the actomyosin network.

bioRxiv preprint doi: https://doi.org/10.1101/2020.05.24.111831; this version posted May 24, 2020. The copyright holder for this preprint (which was not certified by peer review) is the author/funder, who has granted bioRxiv a license to display the preprint in perpetuity. It is made available under aCC-BY-NC-ND 4.0 International license.

How does PCDH7 regulate myosin activity at the cleavage furrow? PCDH7 was previously shown to interact with Protein Phosphatase 2A (PP2A) and SET oncoprotein. The interaction of PCDH7 with PP2A prevents the dephosphorylation of ERK, thus, induces MAPK signaling during lung tumorigenesis (Zhou et al., 2017). Our BioID data revealed that both myosin heavy chain 9 (MYH9) and the regulatory subunit of PP2A (PPP2R1A) are the interaction partners of PCDH7 **(Supplementary Table 1)**. Therefore, it is highly possible that PCDH7 is recruited to the cleavage furrow to regulate the myosin activity by preventing its dephosphorylation by protein phosphatases.

Using two different cell types allowed us to uncover the role of PCDH7 in cytokinesis plasticity. We observed that PCDH7 does not only regulate myosin activity at the cleavage furrow, but also functions in a myosin independent redundant pathway. Unlike Hela S3 cells, adherent cells like RPE1 can perform adhesion-dependent cytokinesis in the absence of a functional actomyosin contractile ring (Dix et al., 2018). In line with the role of PCDH7 during adhesion-dependent cytokinesis, we observed a significant cytokinesis failure in PCDH7 KO RPE1 cells when myosin activity was abolished by blebbistatin treatment **(Figure 6)**. The remodeling of mitotic adhesion assists dividing cells for separation and re-spreading (Dix et al., 2018; Lock et al., 2018). Integrin dependent cell-substrate adhesion has been shown to be the dominant player of cytokinesis in adherent non transformed human cells (Dix et al., 2018). In the absence of a functional actomyosin ring, cells with thick tails that contact cells with the substrate were able to undergo cytokinesis whereas cells without tails tend to fail in cell division. PCDH7 localizes to those thick tails and retraction fibers during mitosis (Video S1), which may play a crucial role in adhesion dependent cytokinesis. Our analysis showed that blocking both integrin mediated adhesion and myosin II caused a strong cytokinesis failure however those two components are not absolutely required for cytokinesis. Strikingly, a substantial proportion of cells were still able to divide under these conditions which was completely dependent on PCDH7. Therefore, we suggest that PCDH7 is part of feedback mechanisms that promote cytokinesis when myosin II-dependent and integrin-mediated adhesion-dependent cytokinesis is blocked. As a protocadherin family member and part of actomyosin complex, PCDH7 may mediate the cross talk between myosin dependent and adhesion-dependent cytokinesis.

In summary, our study attributes a new function to a member of the protocadherin family, PCDH7, in cytokinesis. PCDH7 localizes to the mitotic cortex and the cleavage furrow in a palmitoylation-dependent manner. We addressed the roles of PCDH7 in different mechanisms of cytokinesis: While PCDH7 is required for the accumulation of active myosin at the cleavage furrow during myosin II-dependent cytokinesis (**Figure 7**, left), it provides a complementary

bioRxiv preprint doi: https://doi.org/10.1101/2020.05.24.111831; this version posted May 24, 2020. The copyright holder for this preprint (which was not certified by peer review) is the author/funder, who has granted bioRxiv a license to display the preprint in perpetuity. It is made available under aCC-BY-NC-ND 4.0 International license.

mechanism to the integrin-mediated cell adhesion and assists cell division during adhesion-dependent cytokinesis, (**Figure 7**, right). We suggest that the palmitoylation-dependent targeting of PCDH7 to the cleavage furrow in adherent cells mediates the coordination of these two redundant pathways. Further investigation of the underlying molecular mechanism of cytokinesis plasticity will unravel the fundamental mechanisms existing in human cells by which cytokinesis is adapted under different conditions and will offer new avenues for therapeutic approaches.

MATERIALS AND METHODS

Cell Lines and Culture

HeLa S3 cells (ATCC CCL-2.2, female) and HEK293T cells (a kind gift from Dr. Tamer Önder) were grown in Dulbecco's modified Eagle's medium (DMEM) (Sigma-Aldrich, D6429) supplemented with 1% penicillin-streptomycin (P/S) (Capricorn, PS-B) and 10% fetal bovine serum (FBS) (Gibco, 10270106). PCDH7-BAC-GFP (MCP Ky 5914 T457) (Poser et al., 2008) transgenic cell line was a kind gift from Dr. Ina Poser and were grown in DMEM supplemented with 1% P/S, 10% FBS and 400 µg/ml G418 (Santa Cruz, sc-29065A). RPE1 cells (ATCC CRL-4000, female) were a kind gift from Dr. Elif Nur Fırat-Karalar and grown in DMEM/F-12 medium (Sigma-Aldrich, D6421) supplemented with 1% P/S, 10% FBS and 1% L-Glutamine (Wisent, 609065).

Cell Synchronization

Cells were synchronized to mitosis, interphase (Ozlu et al., 2010) and cytokinesis (Hu et al., 2008; Karayel et al., 2018) as described previously.

Briefly, HeLa S3 cells were incubated with 2 mM thymidine (Santa Cruz, sc-296542) containing media for 20 hours, then released with excessive PBS washes. Fresh complete media was then added and incubated for 8 hours. After the second thymidine block for another 19 hours interphase cells were collected or fixed for immunofluorescence analysis. For monopolar mitosis, cells were released from the second thymidine block by PBS wash and incubated with fresh media containing 10 µM S-trityl-L-cysteine (STC) (Sigma-Aldrich, 164739) for 20 hours. For the monopolar cytokinesis, cells were released from the thymidine block by PBS wash, incubated with fresh media containing 10 µM STC for 16-20 hours, then incubated with 100 µM purvalanol A (Tocris Bioscience, 1580) for 15 minutes. For bipolar synchronization, cells were released from the thymidine block by PBS wash and incubated with 10 ng/ml of

bioRxiv preprint doi: https://doi.org/10.1101/2020.05.24.111831; this version posted May 24, 2020. The copyright holder for this preprint (which was not certified by peer review) is the author/funder, who has granted bioRxiv a license to display the preprint in perpetuity. It is made available under aCC-BY-NC-ND 4.0 International license.

nocodazole (Calbiochem, 487928) for 5 hours. At the end of nocodazole incubation, cells were arrested in mitosis. For cytokinesis, cells were released from mitosis by removal of the nocodazole from the medium and incubated 1 hour in complete medium to collect cytokinesis cells.

Drug Treatments

In order to inhibit the palmitoylation, cells were incubated with 100 µM 2-Bromopalmitate (2BP) (Sigma, 21604) overnight (Webb et al., 2000). In order to inhibit myosin II activity, 100 µM blebbistatin (Santa Cruz, sc204253) was added on cells about 30 minutes before starting the live imaging experiments (Straight et al., 2003). To inhibit the integrin binding, cells were incubated with 1 mM GRGDSP peptide (Anaspec, 22945) for 2 hours (Gilchrist et al., 2007).

Immunostaining and Microscopy

PCDH7-BAC-GFP cells that stably express PCDH7:GFP near physiological levels were used for both live imaging and fixed imaging experiments. For fixed images, GFP signal of PCDH7-BAC-GFP cells was amplified using GFP antibody. For immunostaining, cells were plated on coverslips (12 mm) fixed with 3% paraformaldehyde (PFA), blocked and incubated with primary and secondary antibodies in 2% BSA in PBS containing 0.1% Triton-X. The following antibodies and reagents were used in immunostaining experiments: Tubulin (Cell Signaling, CS2128S), GFP (non-commercial/Invitrogen, A11120), HA (Abcam, ab16918), pMyosin (Cell Signaling, CS3675), Alexa Fluor®-488 and Alexa Fluor®-555 (Cell Signaling), Streptavidin-Alexa Fluor 488 (Invitrogen, S32354), Phalloidin iFlour (Abcam, ab176756), DAPI (Sigma Aldrich, D8417).

Confocal images were taken either by Nikon-Eclipse 90i (EZ-C1 software) confocal microscope using the 60x Plan Apo 1.4 NA oil-immersion objective or by of Leica DMi8/SP8 TCS-DLS (LAS X Software) laser scanning confocal microscope using 40× Plan Apo 1.3 NA oil-immersion objective.

Prior to live cell imaging, cells were plated either on ibiTreat, ibidi µ-Slide 8 Well (ibidi, 80826) or µ-Dish 35 mm (ibidi, 81156) plates. Live imaging experiments were performed using Zeiss Cell Observer SD spinning disk microscope (ZEN Software) with 20x Plan Apo 0.8 NA objective and Leica DMi8 widefield fluorescence microscope (LAS X Software) with 63× Plan Apo 1.4 NA oil immersion objective or 20× PL FLUOTAR L 0.40 NA objective

bioRxiv preprint doi: https://doi.org/10.1101/2020.05.24.111831; this version posted May 24, 2020. The copyright holder for this preprint (which was not certified by peer review) is the author/funder, who has granted bioRxiv a license to display the preprint in perpetuity. It is made available under aCC-BY-NC-ND 4.0 International license.

equipped with 37°C and 5% CO2 chambers. Single images or Z-stacks were acquired every 3 minutes and single focal plane was used in the figures unless specified in the figure legends.

Apart from FRAP data, all images were analyzed in Fiji. Graphs and statistical data were generated in GraphPad Prism. Statistical details of each experiments including the statistical test used, exact value of n and definition error bars can be found in figure legend for each figure.

FRAP

Microscopy setup

The microscopy set-up included a frequency doubled femtosecond-pulsed Ti:Sa solid-state tunable laser source (Chameleon Ultra II, Coherent) equipped with a second harmonic generator. Laser output was tuned to 488 nm and the beam directed through mirrors and a Keplerian telescope to the inverted microscope (Eclipse TE2000-U; Nikon) equipped with a dichroic mirror (Chroma, Q495LP) and 60X oil-immersion objective (Nikon Apo TIRF, NA=1.49). A 300 mm focal length lens was placed right before the microscope to focus laser at the back focal plane of the microscope objective to obtain wide field illumination. Microscope was equipped with two different cameras for brightfield and fluorescence image acquisitions. Brightfield images were captured by a CCD camera (Thorlabs, DCU223M). Fluorescence images were captured by an EMCCD camera (Hamamatsu ImagEM C9100-13) placed after an emission filter with pass band 530 ± 30 nm. Photobleaching was performed by removing the neutral density optical filter and the lens right before the microscope, and simultaneously focusing the laser light at the desired area for a duration of 1 second. FRAP image acquisition was done every five seconds using an automated shutter and minimum 130 frames were captured following photobleaching of each sample.

Data Processing

Image analysis was done by using a MATLAB code based on the double normalization algorithm (Phair et al., 2004). In this method, overall decrease in the fluorescence intensity of the samples is also considered and the normalized intensity of the region of interest (ROI). $I_{normalized}$ is given by:

$$I_{normalized}(t) = \frac{I_{total,\ prebleached} - BG}{I_{bleached\,region,\ prebleached} - BG} \cdot \frac{I_{bleached\,region}(t) - BG}{I_{total}(t) - BG}$$

bioRxiv preprint doi: https://doi.org/10.1101/2020.05.24.111831; this version posted May 24, 2020. The copyright holder for this preprint (which was not certified by peer review) is the author/funder, who has granted bioRxiv a license to display the preprint in perpetuity. It is made available under aCC-BY-NC-ND 4.0 International license.

In which, $I_{total,\ prebleached}$ and $I_{bleached\ region,\ prebleached}$ are prebleached intensities of the whole cell and the ROI, respectively. $I_{bleached\ region}(t)$ and $I_{total}\ (t)$ are corresponding intensities at time t. BG is the intensity of the background region. Total number of frames and the first post bleached frame was defined for each sample. Size of the selected background and the ROI areas in each sample were fixed to 14x14 pixels (Kappel, 2004). Unhealthy cells and the motile cells that obstruct the tracking of the ROI throughout the frames are discharged from the data. Obtained $I_{normalized}(t)$ data for each cell then is fitted to $1 - Ae^{-at} - Be^{-bt}$ (Phair et al., 2004) to get half time values $t_{1/2}$. Recovery percentage was also calculated for each cell. The *Mann–Whitney U test* was applied to reveal statistical differences in the recovery and the half-time between samples. Average recovery curves for each group of cells (cell-cell contacts in interphase and mitotic plasma membrane) were obtained by normalizing all individual recovery graphs recorded within a group to 1 and calculating the average points as well as standard deviations of the recovery data at specified frames (time instances) after photobleaching.

Transfection and Viral Transduction

Transient transfection of cells was performed using polyethylenimine (PEI) or Lipofectamine 2000 protocols (Invitrogen, 11668019). For PEI protocol, transfection mixtures were prepared in Opti-MEM reduced serum medium (Invitrogen,31985047) using PEI with 60 µg DNA in 3:1 ratio. After 30 minutes of incubation at room temperature, transfection mixture was added onto cells that were in fresh complete media. For Lipofectamine 2000 protocol, manufacturer's instructions were fallowed.

For viral transduction, lentiviruses were packaged in HEK293T cells using PEI transfection of target sequence containing vector (pLenti), packaging vector (psPAX2, Addgene 12260) and envelope vector (pVSVg, Addgene 8454). Viral particles were collected after 48 and 72 hours of transfection and used to infect HeLa S3 and RPE1 cells in the presence of 2 µg/µl protamine sulfate (Sigma-Aldrich, P4505) as coadjutant. Transduced cells were then selected with the appropriate selective antibiotic.

BioID

bioRxiv preprint doi: https://doi.org/10.1101/2020.05.24.111831; this version posted May 24, 2020. The copyright holder for this preprint (which was not certified by peer review) is the author/funder, who has granted bioRxiv a license to display the preprint in perpetuity. It is made available under aCC-BY-NC-ND 4.0 International license.

PCDH7 sequence was amplified from PCDH7:eGFPN1 and cloned into BioID vector (pcDNA3.1 MCS-BirA* (R118G) Addgene; 36047). Appropriate restriction enzyme cut sites were introduced during amplification using specific primers: NheI_PCDH7_F 5'-GTCAGCTAGCACCATGCTGAGGATGCGGACC-3', EcoRI_PCDH7_R 5'-GCTAGAATTCGCCCTCCCTGGGATATTTAAATATATTTG-3'.

In order to obtain cell cycle specific proximal interactors, double thymidine/STC synchronization methods were modified for BioID protocol (Roux et al., 2012). Briefly, cells were transfected with BioID vector during the release after the first thymidine block (2 mM) and kept in the transfection media during second thymidine block (2 mM). For interphase cells, cells were incubated with fresh media containing thymidine (2 mM) and 50 µM Biotin (Invitrogen, B20656). For mitosis cells, thymidine was released, and cells were incubated with fresh media containing 10 µM STC and Biotin. Both groups were either fixed for immunostaining or pelleted after 20 hours of incubation.

Cell pellets were lysed in lysis buffer (50 mM Tris, pH 7.4; 500 mM NaCl; 0.4% SDS; 5 mM EDTA; 2% TritonX; 1 mM DTT; Protease Inhibitor) and incubated with Streptavidin beads (Pierce,53117) overnight at 4°C in a tube rotator. Fractions of whole cell lysate (WCL) and Unbound (Ub) were kept at -20°C for further analysis. Beads were washed twice with Wash Buffer 1 (2% SDS in dH_2O), once with Wash Buffer 2 (2% deoxycholate; 1% TritonX; 50 mM NaCl; 50 mM Hepes, pH 7.5; 1 mM EDTA), once with Wash Buffer 3 (0.5% NP-40; 0.5% deoxycholate; 1% TritonX; 500 mM NaCl; 1 mM EDTA; 10 mM Tris, pH 8.1) and once with Wash Buffer 4 (50 mM Tris, pH 7.4; 50 mM NaCl). For Western blot analysis, bound proteins were eluted from the streptavidin beads with 50 µl of Laemmli-DTT sample buffer containing 500 nM D-Biotin at 98°C by centrifugation at 1,000 rpm mixing for 10 minutes. For mass spectrometry analysis, on bead tryptic digestion was performed. Briefly, beads were washed with urea buffer (8 M urea (Sigma-Aldrich, A2383) in 0.1 M Tris/HCl pH 8.5) Then, bead-bounded proteins were reduced with 100 mM Dithiothreitol (DTT) (Sigma-Aldrich, 43815) in urea buffer at 56°C for 30 minutes. After reduction, cysteine residues were alkylated using 100 mM iodoacetamide (Applichem, A1666) in urea buffer with 20 minutes incubation in dark. After alkylation, beads were washed with 50 mM ammonium bicarbonate (Applichem, A3583) and incubated with Trypsin (Thermo Scientific,25247) at 37°C overnight (14-16 hours) in ThermoMixer (Eppendorf™) with 1,000 rpm shaking. Next morning, digested peptides were collected and desalted using C18 STAGE Tips and analyzed in Thermo

bioRxiv preprint doi: https://doi.org/10.1101/2020.05.24.111831; this version posted May 24, 2020. The copyright holder for this preprint (which was not certified by peer review) is the author/funder, who has granted bioRxiv a license to display the preprint in perpetuity. It is made available under aCC-BY-NC-ND 4.0 International license.

Scientific Q-Exactive Orbitrap LC-MS/MS mass spectrometer. Experiment was performed in 4 biological replicates with minimum 2 technical replicates for each.

Mass Spectrometry and Data Analysis

Peptides were analyzed by online C18 nanoflow reversed-phase nLC (NanoLC-II, Thermo Scientific) or C18 nanoflow reversed-phase HPLC (Dionex Ultimate 3000, 3500 RSLC nano, Thermo Scientific) connected with an orbitrap mass spectrometer (Q Exactive Orbitrap, Thermo Scientific). Samples were separated in an in-house packed 100 µm i.d. × 23 cm C18 column (Reprosil-Gold C18, 5 µm, 200 Å, Dr. Maisch) using 80 minute linear gradients from 5-25%, 25-40%, 40-95% acetonitrile in 0.1% formic acid with 300 nL/min flow in 100 minutes total run time. The scan sequence began with an MS1 spectrum (Orbitrap analysis; resolution 70,000; mass range 400–1,500 *m*/*z*; automatic gain control (AGC) target 1e6; maximum injection time 32 ms). Up to 15 of the most intense ions per cycle were fragmented and analyzed in the orbitrap with Data Dependent Acquisition (DDA). MS2 analysis consisted of collision-induced dissociation (higher-energy collisional dissociation (HCD)) (resolution 17,500; AGC 1e6; normalized collision energy (NCE) 26; maximum injection time 85 ms). The isolation window for MS/MS was 2.0 *m*/*z*.

Raw files were processed with Proteome Discoverer 2.3 (Thermo Scientific) software. Carbamidomethylation of cysteine residues was used as fixed modification, and acetylation (protein N-termini) and oxidation of methionine residues were used as variable modifications. Maximal two missed cleavages were allowed for the tryptic peptides. The precursor mass tolerance was set to 10 ppm and fragment mass tolerance was set to 0.02 Da. Both peptide and protein false discovery rates (FDRs) were set to 0.01. The other parameters were used with default settings. The database search was performed against the human Uniprot database (release 2015) containing 21,039 entries using the SEQUEST HT search engine integrated into the Proteome Discoverer environment.

BioID Data processing

The spectral counts of proteins were used to calculate fold change ratios and FDR values for identified proteins using the qspec-param programme of qprot_v1.3.5 (Choi et al., 2015). Proteins are filtered with a 0.05 cut-off for FDR values. Significant protein hits were loaded into the String database v11.0 (Szklarczyk et al., 2019) by Cytoscape

bioRxiv preprint doi: https://doi.org/10.1101/2020.05.24.111831; this version posted May 24, 2020. The copyright holder for this preprint (which was not certified by peer review) is the author/funder, who has granted bioRxiv a license to display the preprint in perpetuity. It is made available under aCC-BY-NC-ND 4.0 International license.

StringApp (Doncheva et al., 2019) with 0.7 confidence. MCODE clustering of the network was performed by Cytoscape (version 3.7.2) and its plugin clustermaker (Cline et al., 2007). GO and KEGG enrichment analysis of the network was performed via g:Profiler (Raudvere et al., 2019).

CRISPR

Single guide RNAs (sgRNAs) that target PCDH7 were designed using online "CRISPR design toll" (http://crispr.mit.edu). The following oligonucleotide sequences were used as top/bottom pairs: sg1 5'-CACCGCGACGTCCGCATCGGCAACG-3'/5'-AAACCGTTGCCGATGCGGACGTCG-3', sg2 5'-CACCGTTGCCGATGCGGACGTCGGC-3'/5'-AAACGCCGACGTCCGCATCGGCAA-3', sg5 5'-CACCGCATCGTGACCGGATCGGGTG-3'/5'-AAACCACCCGATCCGGTCACGATG-3', sg6 5'-CACCGCGGGCTTCTCTTTGGCGCGC-3'/5'-AAACGCGCGCCAAAGAGAAGCCCGC-3'. All sgRNAs were cloned into lentiCRISPR plasmid (Shalem et al., 2014) (pXPR_001, 49535, Addgene) as described in (Ran et al., 2013).

PCDH7 knockout cell lines were generated by lipofectamine transfection of CRISPR plasmid to HeLa S3 and RPE1 cells followed by antibiotic selection. Single colonies were isolated with serial dilution of the pool population and PCDH7 knockout clones were selected after verifying the absence of PCDH7 protein expression with Western blot. CRISPR rescue cell lines were generated by viral transduction of pLenti (Campeau et al., 2009) PCDH7:eGFP plasmid to PCDH7 knockout cells.

Western Blot

Samples were separated by molecular weight using 10% SDS-PAGE gels and transferred to a nitrocellulose membrane. The membrane was blocked with 4% w/v nonfat dry milk in TBS-0.1% Tween-20 and probed with 1 µg/ml of the described primary antibody diluted in 2% BSA TBS-0.1% Tween-20. The signal was visualized using ECL (Pierce, 32106) detection of the HRP-conjugated secondary antibodies (Cell Signaling, 7074S, 70765). The following primary antibodies were used in the Western blot analysis: PCDH7 (Abcam, ab139274), EGFR (Santa Cruz, SC-03), Tubulin (Cell Signaling, 3873), Actin (Abcam, ab6276), Phospho-Histone H3 (Upstate; 06-570) and Biotin (non-commercial).

bioRxiv preprint doi: https://doi.org/10.1101/2020.05.24.111831; this version posted May 24, 2020. The copyright holder for this preprint (which was not certified by peer review) is the author/funder, who has granted bioRxiv a license to display the preprint in perpetuity. It is made available under aCC-BY-NC-ND 4.0 International license.

Surface Labelling and Pulldown of Cell Surface Proteins

Plasma membrane proteins were labelled with sulfo-NHS-SS-biotin for membrane enrichment as previously described (Ozkan Kucuk et al., 2018). Briefly, cells were incubated with 5 mM S-NHS-SS-biotin (Pierce, 21331) for 30 minutes at 4°C with gentle shaking, reaction was quenched with glycine and cells were snap frozen. Cells were lysed in a buffer (10 mM TrisCl pH 7.6, 0.5% SDS, 2% NP40, 150 mM NaCl, 1 mM EDTA, 10 mM Iodoacetamide) supplemented with protease inhibitors (Pierce, 88666) and lysates were incubated with pre-conditioned Streptavidin Plus UltraLink Resin (Pierce, 53117) overnight at 4°C. Unbound samples were collected and beads were washed with lysis buffer three times. Biotinylated surface proteins were eluted by boiling at 70°C for 20 minutes in SDS sample buffer including 100 mM DTT with agitation. All fractions including whole cell lysate (Input-I), unbound (U) and plasma membrane enriched (Elute-E) were analyzed by Western blot.

Triton X-114 Extraction

Hydrophobic proteins were extracted from the hydrophilic ones using the Triton X-114 extraction protocol as described (Bordier, 1981; Taguchi et al., 2013). Briefly, first precondensation of the Triton X-114 was performed by repeated cycles of clarifying at 4°C and incubation at 37°C to separate the detergent phase. Cells were lysed using 2% TX114 lysis buffer in PBS and lysate was cleared by centrifugation at 16,100 g for 3 minutes at 4°C. Lysate was then centrifuged at 22,000 g for 10 minutes at room temperature for phase separation. The aqueous phase was removed, detergent phase was washed with 0.1% TX114 wash buffer and clarified on ice and incubated at 37°C for phase separation. Centrifugation and washing steps were repeated 2 more times and detergent and aqueous phases were collected for further analysis.

AUTHOR CONTRIBUTIONS

N.E.Ö. designed and performed the experiments, analyzed the data, and wrote the manuscript. M.H.Q. designed and created CRISPR knockout cell lines and PCDH7:GFP constructs. B.N.Y. performed experiments together with N.E.Ö. A.K. analyzed the BioID data. N.B. performed FRAP experiments together with N.E.Ö and analyzed the FRAP data. A.K. designed and analyzed FRAP experiments. N.Ö. designed the research, provided funding, and wrote the manuscript.

bioRxiv preprint doi: https://doi.org/10.1101/2020.05.24.111831; this version posted May 24, 2020. The copyright holder for this preprint (which was not certified by peer review) is the author/funder, who has granted bioRxiv a license to display the preprint in perpetuity. It is made available under aCC-BY-NC-ND 4.0 International license.

ACKNOWLEDGMENTS

This study is funded by TUBITAK 1001 (116Z305) to N.Ö. We gratefully acknowledge Büşra Akarlar and the Proteomics Facility of Koç University for the technical assistance in mass spectrometry analyses. We thank Dr. Bilal Ersan Kerman and Medipol University Regenerative and Restorative Medicine Research Centre for the permission to use their imaging facility and for the critical discussions throughout the project. İlayda Aydınlı and Tuba Oğuz for their assistance during live imaging experiments. We also thank Dr. Alexandr Jonas for the critical discussions and interpretations of FRAP data. We thank Dr. Timothy Mitchison for the anti-biotin antibody and the critical reading of the manuscript. We also thank Dr. Nazan Saner and Aydanur Şentürk for the critical reading of the manuscript. We gratefully acknowledge the permission to use the facilities of the Cellular and Molecular Imaging Core of Koç University Research Center for Translational Medicine funded by the Republic of Turkey Ministry of Development.

COMPETING INTERESTS

The authors declare no competing interests.

bioRxiv preprint doi: https://doi.org/10.1101/2020.05.24.111831; this version posted May 24, 2020. The copyright holder for this preprint (which was not certified by peer review) is the author/funder, who has granted bioRxiv a license to display the preprint in perpetuity. It is made available under aCC-BY-NC-ND 4.0 International license.

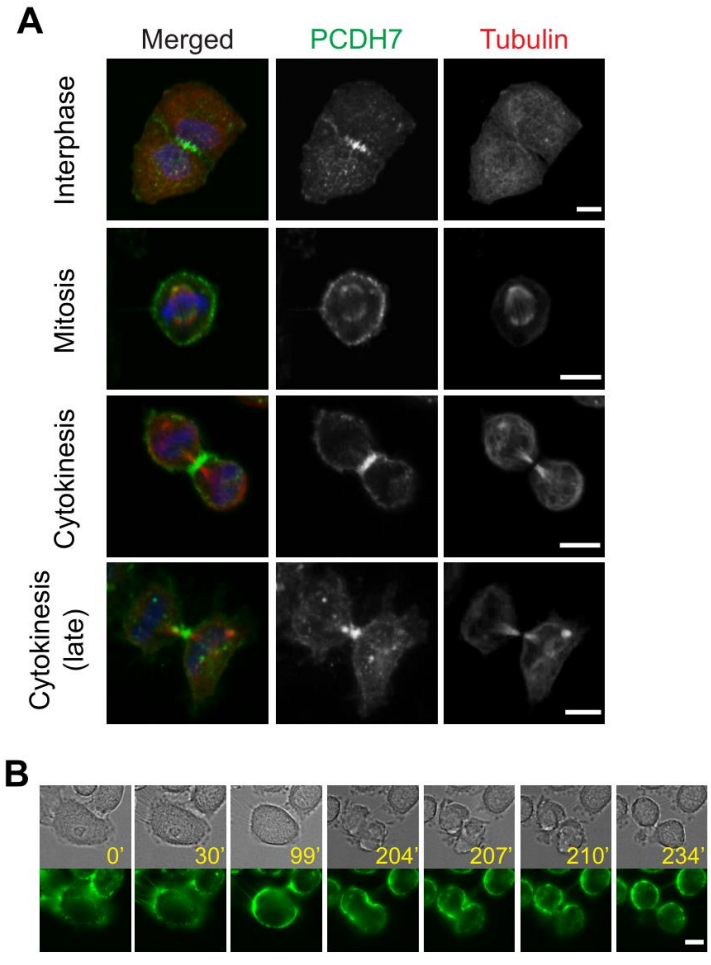

Figure1. Subcellular localization of PCDH7 during cell division.
A. Fluorescence images show the subcellular localization of PCDH7 (green), Microtubules (α-Tubulin) (red) and DNA (blue) in fixed PCDH7-BAC-GFP cells during interphase, mitosis and cytokinesis. **B.** Live imaging snapshots of HeLa S3-PCDH7:GFP cells during cell division. Upper panel, bright field; lower panel, fluorescence imaging. Relative timing is shown in minutes. Scale bars: 10 μm.

bioRxiv preprint doi: https://doi.org/10.1101/2020.05.24.111831; this version posted May 24, 2020. The copyright holder for this preprint (which was not certified by peer review) is the author/funder, who has granted bioRxiv a license to display the preprint in perpetuity. It is made available under aCC-BY-NC-ND 4.0 International license.

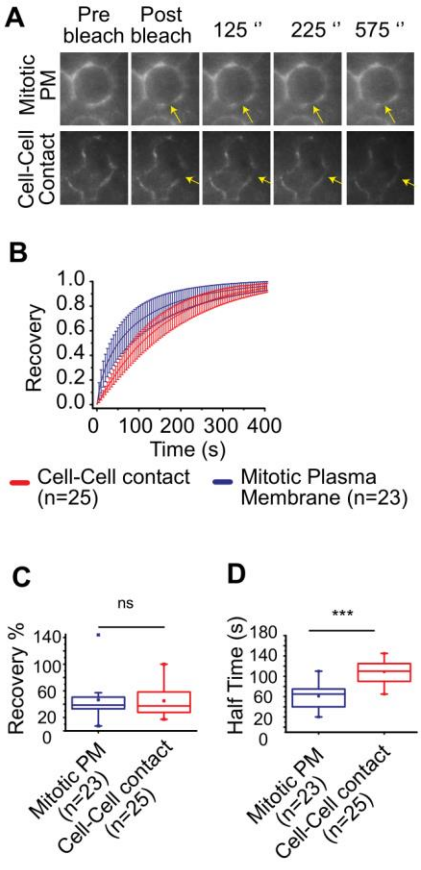

Figure2. FRAP analysis reveals the dynamic localization of PCDH7 to the plasma membrane.
A. Representative images for mitotic plasma membrane (upper panel) and cell-cell contact (lower panel) localization of PCDH7 during FRAP analysis. Yellow arrows indicate the bleached area. **B.** Recovery curve of PCDH7 in mitotic plasma membrane (blue) and cell-cell contact regions (red) after photobleaching. **C.** Comparison of recovery levels in mitotic plasma membrane (blue) and cell-cell contact regions (red). Statistics used *Mann–Whitney U test.* **D**. Comparison of recovery halftimes in mitotic plasma membrane (blue) and cell-cell contact regions (red). Statistics used *Mann–Whitney U test.*
N represents the number of the cells analyzed. ***: $p<0.001$, ns: non-significant.

bioRxiv preprint doi: https://doi.org/10.1101/2020.05.24.111831; this version posted May 24, 2020. The copyright holder for this preprint (which was not certified by peer review) is the author/funder, who has granted bioRxiv a license to display the preprint in perpetuity. It is made available under aCC-BY-NC-ND 4.0 International license.

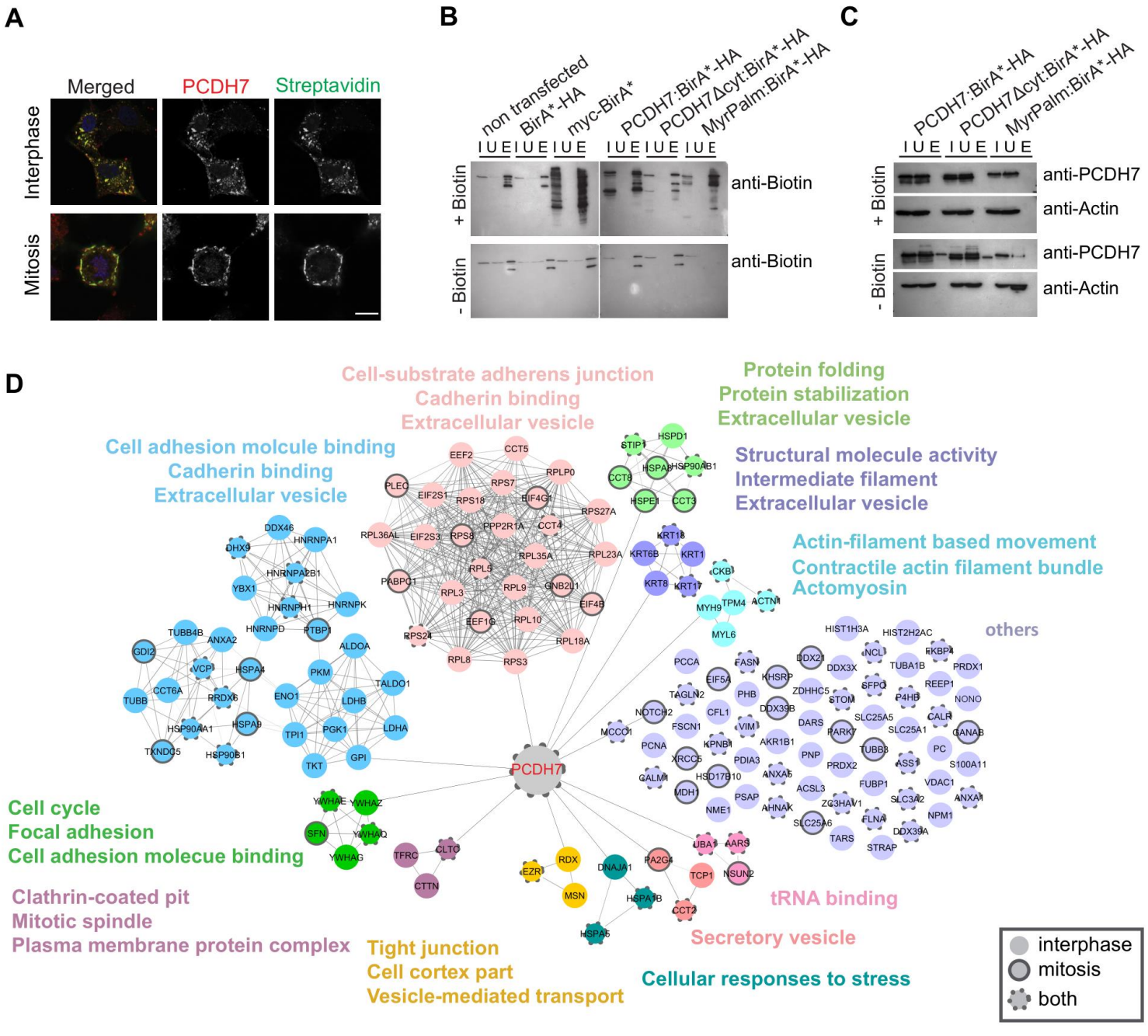

Figure3. Cell cycle stage specific proximity interactome of PCDH7

A. The cell cycle specific localization of PCDH7:BirA*-HA in interphase (upper panel) and mitosis (lower panel) cells, fixed and stained with PCDH7 antibody (red) and fluorescence conjugated streptavidin (green), DAPI in blue. **B.** Western blotting analysis shows the biotinylation efficiency of BioID constructs. Controls; non transfected, backbone vector transfected (BirA*-HA and mycBirA*). Samples; PCDH7:BirA*-HA, PCDH7Δcyt:BirA*-HA, myrPalm:BirA*-HA (an unrelated construct as negative control). Upper blot; Cells supplied with biotin. Lower blot; Cells not supplied with biotin. **C.** Western blotting analysis shows the biotinylation specificity of BioID constructs. Upper blot; Cells supplied with biotin. Lower blot; Cells not supplied with biotin. Both PCDH7 and truncated PCDH7 (PCDH7Δcyt) are enriched in the elute fractions (E) after streptavidin pulldown only in the biotin supplied cells (upper panel). No PCDH7 enrichment is observed in the negative control. **D.** Mapping the proximity interaction networking of PCDH7. Different colors represent the significantly enriched clusters after GO and KEGG enrichment analysis. Interphase specific interactions are represented with non-bordered nodes, mitosis specific interactors are presented in bordered nodes and common interactors are presented with dashed-bordered nodes.
Scale bar: 10 µm, I: Input, U: Unbound, E: Elute.

bioRxiv preprint doi: https://doi.org/10.1101/2020.05.24.111831; this version posted May 24, 2020. The copyright holder for this preprint (which was not certified by peer review) is the author/funder, who has granted bioRxiv a license to display the preprint in perpetuity. It is made available under aCC-BY-NC-ND 4.0 International license.

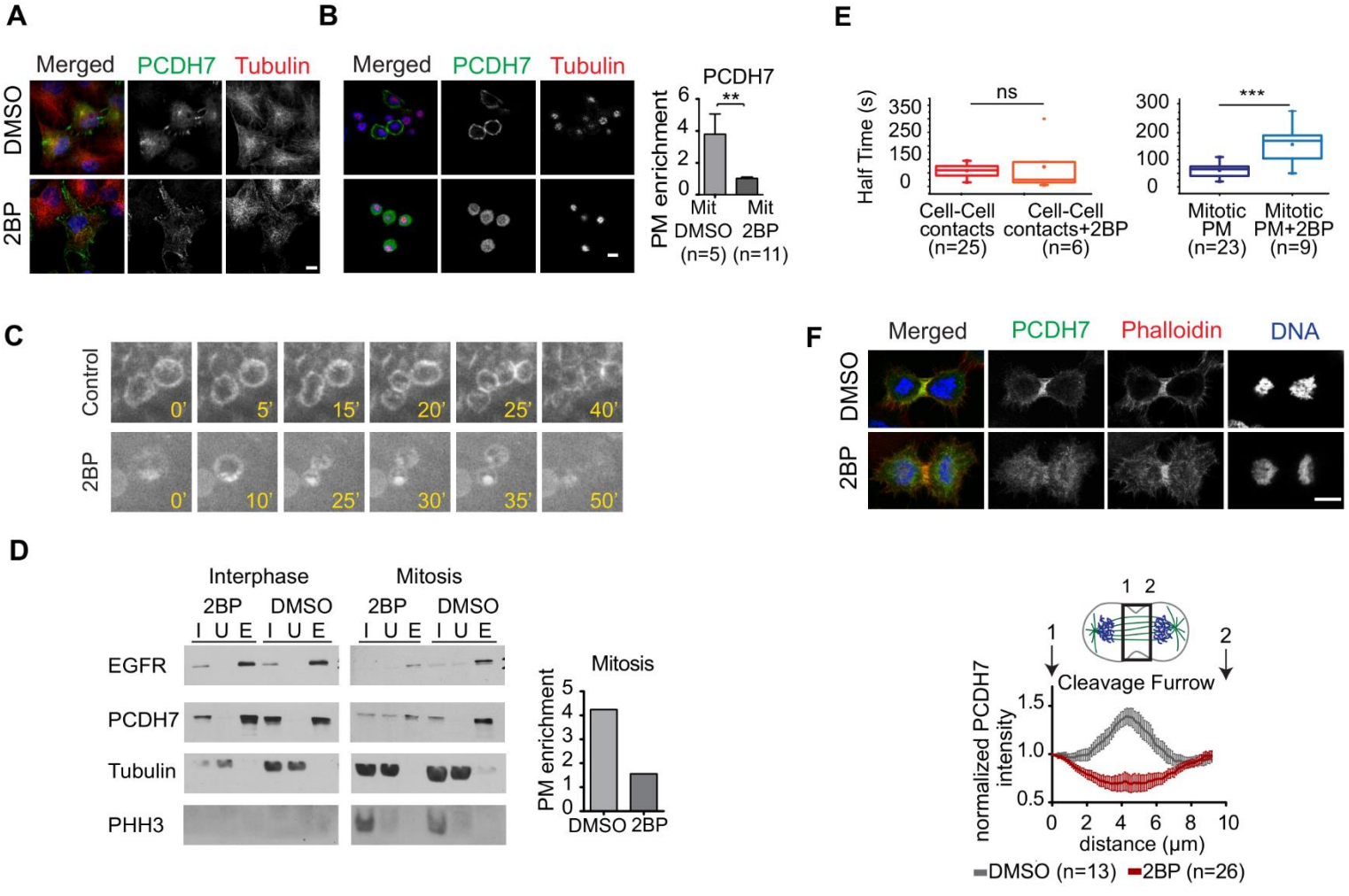

Figure4. Palmitoylation-dependent plasma membrane localization of PCDH7

A. PCDH7 (green) localization during interphase in control (DMSO) (top) and palmitoylation inhibitor, 2BP treated (bottom) cells those are stably expressing PCDH7-BAC-GFP. Microtubules (α-Tubulin) are shown in red and DNA in blue. **B.** PCDH7 (green) localization during mitosis in control (DMSO) (top) and palmitoylation inhibitor, 2BP treated (bottom) cells those are stably expressing PCDH7-BAC-GFP. Cells are synchronized to monopolar mitosis. Microtubules (α-Tubulin) are shown in red and DNA in blue (left). Quantification of the plasma membrane enrichment of PCDH7 during mitosis in the control and 2BP treated cells (right). Statistics used *t test*, error bars: SEM **C.** Live imaging snapshots of the dividing PCDH7-BAC-GFP expressing cells in the control (top panel) and 2BP treated (bottom panel) cells. Relative timing is shown in minutes. **D.** Western blotting analysis of the effect of 2BP on plasma membrane localization of PCDH7. Plasma membrane proteins were labeled with amine reactive biotin and pulled down by streptavidin beads. All fractions (I: Input, U: Unbound, E: Elute) were blotted against EGFR (as a cell surface marker), tubulin (as a cytoplasmic marker) and phospho Histone H3 (as a mitotic marker) (left). The quantification of the plasma membrane enrichment of PCDH7 in the control (DMSO) and 2BP treated mitotic cells (right). **E.** FRAP analysis of PCDH7 in palmitoylation inhibitor 2BP treated cells in comparison to control. The effect of 2BP on recovery half-time of the PCDH7 in cell-cell contacts (left). The effect of 2BP on recovery half-time of the PCDH7 in mitotic plasma membrane (right). Statistics used *Mann–Whitney U test.* **F.** Representative maximum intensity projections of Z-stacks show PCDH7 (green) localization at the cleavage furrow during cytokinesis in PCDH7-BAC-GFP expressing cells. Actin filaments (Phalloidin) are shown in red and DNA in blue (top). Quantification of PCDH7 localization at the cleavage furrow during cytokinesis in the control (gray trace) and 2BP treated (red trace) cells (bottom). Intensity profiles were obtained in ImageJ software for the indicated region of interest as previously described (Uretmen Kagiali et al., 2020).

Scale bars: 10 µm, N represents the number of analyzed cells. **:. $p<0.01$; ***: $p<0.001$ ns: non-significant.

bioRxiv preprint doi: https://doi.org/10.1101/2020.05.24.111831; this version posted May 24, 2020. The copyright holder for this preprint (which was not certified by peer review) is the author/funder, who has granted bioRxiv a license to display the preprint in perpetuity. It is made available under aCC-BY-NC-ND 4.0 International license.

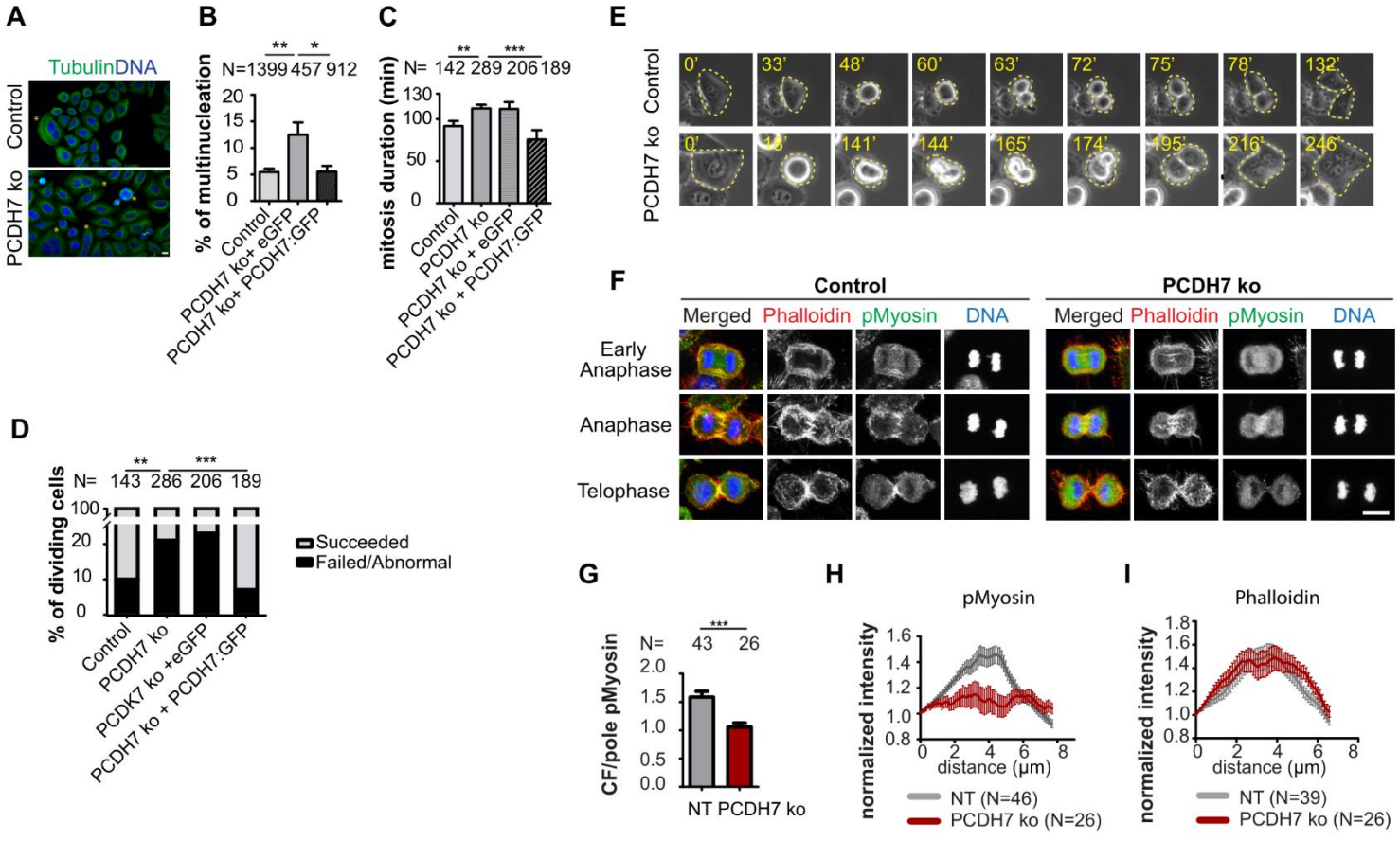

Figure5. Knockout of PCDH7 leads to multinucleated cells

A. Representative fluorescence images of control cells treated with non-targeting sgRNA (sgNT) (upper panel) and PCDH7 knockout HeLa S3 cells (lower panel). Cells were stained with anti-α-tubulin antibody (green) and DAPI for DNA (blue). Yellow asterisks indicate the multinucleated cells. **B.** Quantification of multinucleation percentages of control, PCDH7 knockout (+backbone vector eGFP) and rescue cells (+ PCDH7:eGFP). Statistics used *t test*, error bars: SEM **C.** Comparison of the mitosis duration in control, PCDH7 knockout and rescue cells. Mitosis duration is calculated as the time from cell rounding until the initiation of cleavage furrow formation or until cells fail division. Statistics used *t-test*, error bars: SEM **D.** The quantification of abnormal/failed cell division percentages of control, PCDH7 knockout and rescue cells. Statistics used *Fisher's exact test.* **E.** Representative live imaging snapshots of cell division in control cells (upper panel) and PCDH7 knockout cells (lower panel). Dashed lines indicate cell's margins. Relative timing is shown in minutes. **F.** Fluorescence images displaying phospho-myosin II (S19) (green), actin filaments (Phalloidin, red) and DNA (DAPI, blue) localization through cytokinesis in control (left) and PCDH7 knockout (right) cells. Maximum intensity projections of Z stacks are shown. **G.** Quantification of the average phospho-myosin II intensity enrichment at the cleavage furrow ($Intensity_{Cleavege\ Furrow}$ / $Intensity_{Pole}$) in control (NT) and PCDH7 knockout cells. Statistics used *t test*, error bars: SEM **H.** Comparison of the phospho-myosin II localization at the cleavage furrow in control (gray) and PCDH7 knock out (red) cells. **I.** Comparison of the F-actin (Phalloidin) levels at the cleavage furrow in control (gray) and PCDH7 knock out (red) cells.

Scale bars: 10 μm, N represents the number of the cells analyzed. *: p<0.05; **: p<0.01; ***: p<0.001.

bioRxiv preprint doi: https://doi.org/10.1101/2020.05.24.111831; this version posted May 24, 2020. The copyright holder for this preprint (which was not certified by peer review) is the author/funder, who has granted bioRxiv a license to display the preprint in perpetuity. It is made available under aCC-BY-NC-ND 4.0 International license.

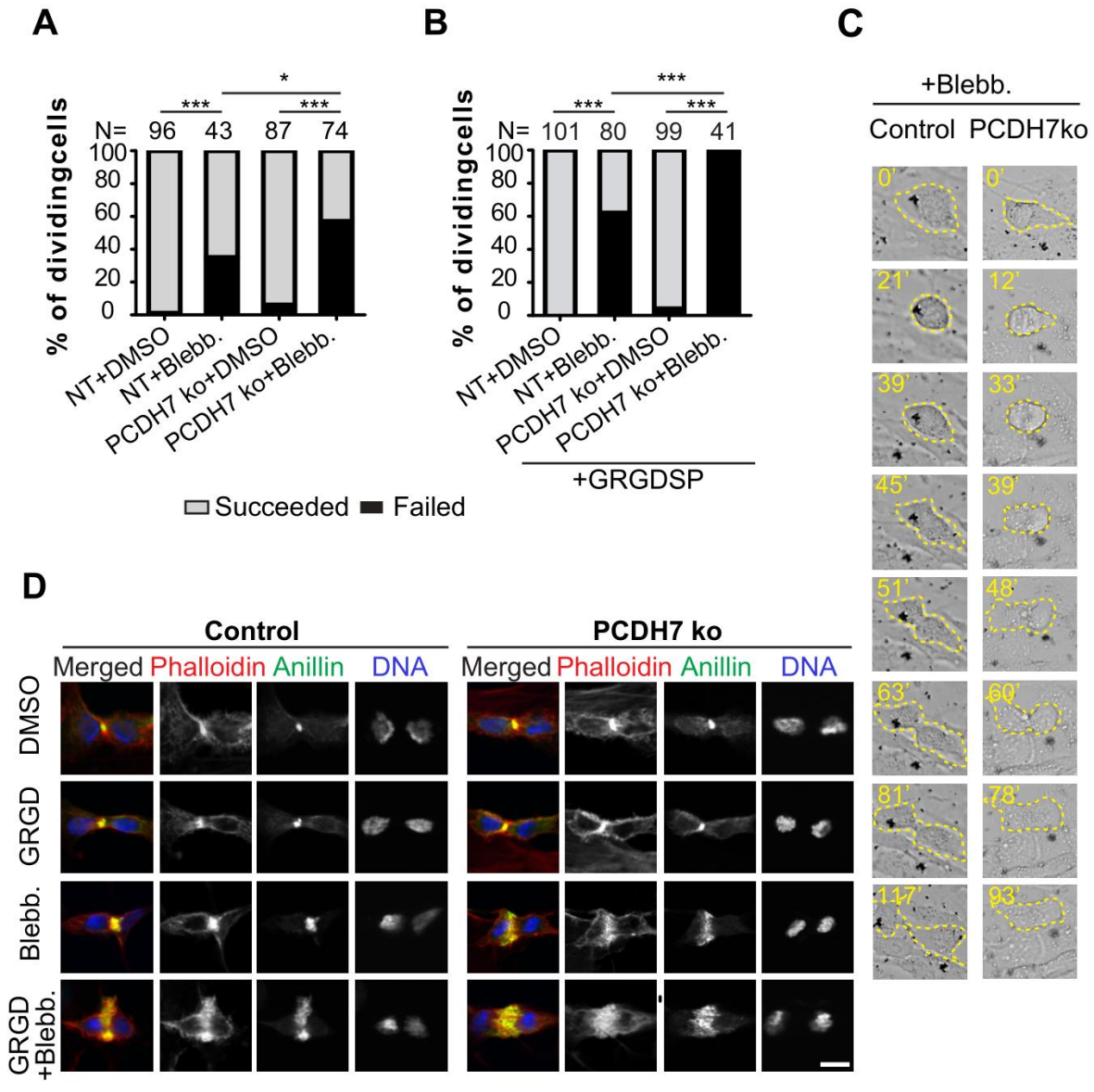

Figure 6. Role of PCDH7 in adhesion-dependent cytokinesis.

A. Quantification of the percentage of cell division failures in control and PCDH7 knockout RPE1 cells treated with DMSO (control) or myosin II inhibitor (+Blebbistatin). Statistics used *Fisher's exact test.* **B**. Quantification of the percentage of cell division failures in control and PCDH7 knockout RPE1 cells treated with DMSO (control) or myosin II inhibitor (+Blebbistatin), when integrin binding is inhibited using GRGDSP peptide. Statistics used *Fisher's exact test.* **C.** Representative live imaging snapshots displaying the effect of myosin II inhibition in RPE1 control cells (left) and PCDH7 knockout cells (right). Dashed lines indicate the cell's margins. Relative timing is shown in minutes. **D.** Representative fluorescence images of DMSO (control, top row), GRGDSP (inhibition of integrin binding, second row), Blebbistatin (inhibition of myosin II, third row) and both GRGDSP and Blebbistatin (inhibition of myosin II and integrin binding, bottom row) treated cells in control (left panel) and PCDH7 knock out (right panel) RPE1 cells. Maximum intensity projections of Z-stacks show actin filaments (Phalloidin, red), anillin (green) and DNA staining (DAPI, blue).

Scale bar: 10 µm, N represents the number of the cells analyzed. *: $p<0.05$; ***: $p<0.0001$.

bioRxiv preprint doi: https://doi.org/10.1101/2020.05.24.111831; this version posted May 24, 2020. The copyright holder for this preprint (which was not certified by peer review) is the author/funder, who has granted bioRxiv a license to display the preprint in perpetuity. It is made available under aCC-BY-NC-ND 4.0 International license.

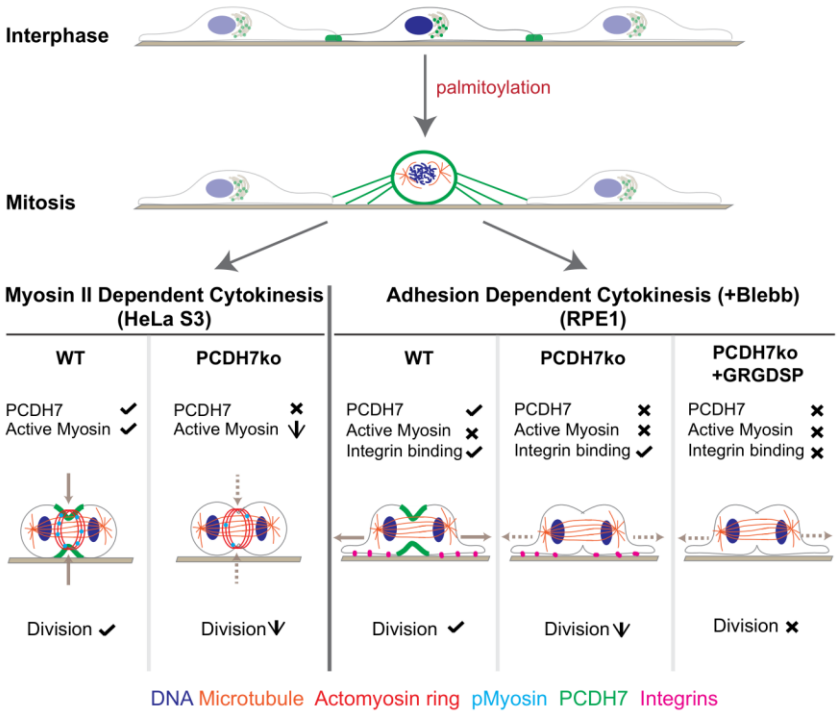

Figure 7. A model describing versatile roles of PCDH7 in cytokinesis

In interphase cells, PCDH7 localizes to cell-cell contacts and endoplasmic reticulum. As cells progress into mitosis, PCDH7 translocates to the plasma membrane in a palmitoylation-dependent manner. During cytokinesis, PCDH7 localizes to the cleavage furrow and regulates myosin II activity. Absence of PCDH7 causes decreased activity of myosin II and an increase in multinucleation. RPE1 cells can perform adhesion-dependent cytokinesis when myosin II activity is inhibited. Absence of PCDH7 perturbs this ability and increases cytokinesis failure. Inhibition of integrin dependent cell adhesion causes an additive effect and almost complete failure in cytokinesis.

bioRxiv preprint doi: https://doi.org/10.1101/2020.05.24.111831; this version posted May 24, 2020. The copyright holder for this preprint (which was not certified by peer review) is the author/funder, who has granted bioRxiv a license to display the preprint in perpetuity. It is made available under aCC-BY-NC-ND 4.0 International license.

CONTACT FOR REAGENT AND RESOURCE SHARING

Further information and requests for resources and reagents should be directed to and will be fulfilled by the Lead Contact, Nurhan Özlü (nozlu@ku.edu.tr).

All unique/stable reagents and codes generated in this study are available from the Lead Contact without restriction.

SUPPLEMENTAL ITEMS

Figure S1. Related to Figure 4.

Figure S2. Related to Figure 5 and Figure 6.

Video S1. Related to Figure 1. Live imaging video of HeLa S3-PCDH7:GFP cells during cell division. Left panel; bright field. Right panel; GFP.

Video S2. Related to Figure 4. Live imaging video of PCDH7-BAC-GFP expressing control (left) and palmitoylation inhibitor 2BP treated (right) cells during cell division.

Video S3. Related to Figure 5. Live imaging video of CRISPR HeLa S3 cells during cell division; sgNT Control, PCDH7 knockout (PCDH7 ko), PCDH7 rescue (PCDH7 ko+PCDH7:GFP) and mock rescue (PCDK7 ko+eGFP).

Video S4. Related to Figure 6A. Live imaging video of CRISPR RPE1 cells; Control cells treated with DMSO (NT+DMSO), Control cells treated with blebbistatin (NT+Blebb), PCDH7 knockout cells threated with DMSO (PCDH7ko+DMSO), PCDH7 knockout cells threated with blebbistatin (PCDH7ko+Blebb).

Video S5. Related to Figure 6B. Live imaging video of CRISPR RPE1 cells treated with GRGDS peptide; Control cells treated with DMSO (NT+GRGD+DMSO), Control cells treated with blebbistatin (NT+GRGD+Blebb), PCDH7 knockout cells treated with DMSO (PCDH7ko+GRGD+DMSO), PCDH7 knockout cells treated with blebbistatin (PCDH7ko+GRGD+Blebb).

Table S1. Related to Figure 3D.

bioRxiv preprint doi: https://doi.org/10.1101/2020.05.24.111831; this version posted May 24, 2020. The copyright holder for this preprint (which was not certified by peer review) is the author/funder, who has granted bioRxiv a license to display the preprint in perpetuity. It is made available under aCC-BY-NC-ND 4.0 International license.

REFERENCES

Blaskovic, S., Blanc, M., and van der Goot, F.G. (2013). What does S-palmitoylation do to membrane proteins? FEBS J *280*, 2766-2774.
Bordier, C. (1981). Phase separation of integral membrane proteins in Triton X-114 solution. J Biol Chem *256*, 1604-1607.
Bradley, R.S., Espeseth, A., and Kintner, C. (1998). NF-protocadherin, a novel member of the cadherin superfamily, is required for Xenopus ectodermal differentiation. Curr Biol *8*, 325-334.
Brownlee, C., and Heald, R. (2019). Importin alpha Partitioning to the Plasma Membrane Regulates Intracellular Scaling. Cell *176*, 805-815 e808.
Campeau, E., Ruhl, V.E., Rodier, F., Smith, C.L., Rahmberg, B.L., Fuss, J.O., Campisi, J., Yaswen, P., Cooper, P.K., and Kaufman, P.D. (2009). A versatile viral system for expression and depletion of proteins in mammalian cells. PLoS One *4*, e6529.
Chen, X., Molino, C., Liu, L., and Gumbiner, B.M. (2007). Structural elements necessary for oligomerization, trafficking, and cell sorting function of paraxial protocadherin. J Biol Chem *282*, 32128-32137.
Choi, H., Kim, S., Fermin, D., Tsou, C.C., and Nesvizhskii, A.I. (2015). QPROT: Statistical method for testing differential expression using protein-level intensity data in label-free quantitative proteomics. J Proteomics *129*, 121-126.
Cline, M.S., Smoot, M., Cerami, E., Kuchinsky, A., Landys, N., Workman, C., Christmas, R., Avila-Campilo, I., Creech, M., Gross, B., *et al.* (2007). Integration of biological networks and gene expression data using Cytoscape. Nat Protoc *2*, 2366-2382.
Cramer, L.P., and Mitchison, T.J. (1997). Investigation of the mechanism of retraction of the cell margin and rearward flow of nodules during mitotic cell rounding. Mol Biol Cell *8*, 109-119.
Dix, C.L., Matthews, H.K., Uroz, M., McLaren, S., Wolf, L., Heatley, N., Win, Z., Almada, P., Henriques, R., Boutros, M., *et al.* (2018). The Role of Mitotic Cell-Substrate Adhesion Re-modeling in Animal Cell Division. Dev Cell *45*, 132-145 e133.
Doncheva, N.T., Morris, J.H., Gorodkin, J., and Jensen, L.J. (2019). Cytoscape StringApp: Network Analysis and Visualization of Proteomics Data. J Proteome Res *18*, 623-632.
Eggert, U.S., Mitchison, T.J., and Field, C.M. (2006). Animal cytokinesis: from parts list to mechanisms. Annu Rev Biochem *75*, 543-566.
Field, C.M., and Alberts, B.M. (1995). Anillin, a contractile ring protein that cycles from the nucleus to the cell cortex. J Cell Biol *131*, 165-178.
Fukata, Y., and Fukata, M. (2010). Protein palmitoylation in neuronal development and synaptic plasticity. Nat Rev Neurosci *11*, 161-175.
Gilchrist, C.L., Chen, J., Richardson, W.J., Loeser, R.F., and Setton, L.A. (2007). Functional integrin subunits regulating cell-matrix interactions in the intervertebral disc. J Orthop Res *25*, 829-840.
Hu, C.K., Coughlin, M., Field, C.M., and Mitchison, T.J. (2008). Cell polarization during monopolar cytokinesis. J Cell Biol *181*, 195-202.
Kahr, I., Vandepoele, K., and van Roy, F. (2013). Delta-protocadherins in health and disease. Prog Mol Biol Transl Sci *116*, 169-192.
Kanada, M., Nagasaki, A., and Uyeda, T.Q. (2005). Adhesion-dependent and contractile ring-independent equatorial furrowing during cytokinesis in mammalian cells. Mol Biol Cell *16*, 3865-3872.
Kappel, C.a.R.E. (2004). Fluorescence recovery after photobleaching with the Leica TCS SP2. Confocal Appl Lett *18*, 1-12.
Karayel, O., Sanal, E., Giese, S.H., Uretmen Kagiali, Z.C., Polat, A.N., Hu, C.K., Renard, B.Y., Tuncbag, N., and Ozlu, N. (2018). Comparative phosphoproteomic analysis reveals signaling networks regulating monopolar and bipolar cytokinesis. Sci Rep *8*, 2269.
Kim, S.H., Yamamoto, A., Bouwmeester, T., Agius, E., and Robertis, E.M. (1998). The role of paraxial protocadherin in selective adhesion and cell movements of the mesoderm during Xenopus gastrulation. Development *125*, 4681-4690.
Kuroda, H., Inui, M., Sugimoto, K., Hayata, T., and Asashima, M. (2002). Axial protocadherin is a mediator of prenotochord cell sorting in Xenopus. Dev Biol *244*, 267-277.

bioRxiv preprint doi: https://doi.org/10.1101/2020.05.24.111831; this version posted May 24, 2020. The copyright holder for this preprint (which was not certified by peer review) is the author/funder, who has granted bioRxiv a license to display the preprint in perpetuity. It is made available under aCC-BY-NC-ND 4.0 International license.

Lancaster, O.M., Le Berre, M., Dimitracopoulos, A., Bonazzi, D., Zlotek-Zlotkiewicz, E., Picone, R., Duke, T., Piel, M., and Baum, B. (2013). Mitotic rounding alters cell geometry to ensure efficient bipolar spindle formation. Dev Cell *25*, 270-283.
Linder, M.E., and Deschenes, R.J. (2007). Palmitoylation: policing protein stability and traffic. Nat Rev Mol Cell Biol *8*, 74-84.
Lock, J.G., Jones, M.C., Askari, J.A., Gong, X., Oddone, A., Olofsson, H., Goransson, S., Lakadamyali, M., Humphries, M.J., and Stromblad, S. (2018). Reticular adhesions are a distinct class of cell-matrix adhesions that mediate attachment during mitosis. Nat Cell Biol *20*, 1290-1302.
Macia, E., Ehrlich, M., Massol, R., Boucrot, E., Brunner, C., and Kirchhausen, T. (2006). Dynasore, a cell-permeable inhibitor of dynamin. Dev Cell *10*, 839-850.
Matsumura, F., Ono, S., Yamakita, Y., Totsukawa, G., and Yamashiro, S. (1998). Specific localization of serine 19 phosphorylated myosin II during cell locomotion and mitosis of cultured cells. J Cell Biol *140*, 119-129.
Mitchison, T.J., and Salmon, E.D. (2001). Mitosis: a history of division. Nat Cell Biol *3*, E17-21.
Morishita, H., and Yagi, T. (2007). Protocadherin family: diversity, structure, and function. Curr Opin Cell Biol *19*, 584-592.
Nagasaki, A., Kanada, M., and Uyeda, T.Q. (2009). Cell adhesion molecules regulate contractile ring-independent cytokinesis in Dictyostelium discoideum. Cell Res *19*, 236-246.
Nigg, E.A. (2001). Mitotic kinases as regulators of cell division and its checkpoints. Nat Rev Mol Cell Biol *2*, 21-32.
Nollet, F., Kools, P., and van Roy, F. (2000). Phylogenetic analysis of the cadherin superfamily allows identification of six major subfamilies besides several solitary members. J Mol Biol *299*, 551-572.
Normand, G., and King, R.W. (2010). Understanding cytokinesis failure. Adv Exp Med Biol *676*, 27-55.
Nurse, P. (1990). Universal control mechanism regulating onset of M-phase. Nature *344*, 503-508.
Ozkan Kucuk, N.E., Sanal, E., Tan, E., Mitchison, T., and Ozlu, N. (2018). Labeling Carboxyl Groups of Surface-Exposed Proteins Provides an Orthogonal Approach for Cell Surface Isolation. J Proteome Res *17*, 1784-1793.
Ozlu, N., Monigatti, F., Renard, B.Y., Field, C.M., Steen, H., Mitchison, T.J., and Steen, J.J. (2010). Binding partner switching on microtubules and aurora-B in the mitosis to cytokinesis transition. Mol Cell Proteomics *9*, 336-350.
Ozlu, N., Qureshi, M.H., Toyoda, Y., Renard, B.Y., Mollaoglu, G., Ozkan, N.E., Bulbul, S., Poser, I., Timm, W., Hyman, A.A., *et al.* (2015). Quantitative comparison of a human cancer cell surface proteome between interphase and mitosis. EMBO J *34*, 251-265.
Phair, R.D., Gorski, S.A., and Misteli, T. (2004). Measurement of dynamic protein binding to chromatin in vivo, using photobleaching microscopy. Methods Enzymol *375*, 393-414.
Poser, I., Sarov, M., Hutchins, J.R., Heriche, J.K., Toyoda, Y., Pozniakovsky, A., Weigl, D., Nitzsche, A., Hegemann, B., Bird, A.W., *et al.* (2008). BAC TransgeneOmics: a high-throughput method for exploration of protein function in mammals. Nat Methods *5*, 409-415.
Ran, F.A., Hsu, P.D., Wright, J., Agarwala, V., Scott, D.A., and Zhang, F. (2013). Genome engineering using the CRISPR-Cas9 system. Nat Protoc *8*, 2281-2308.
Raudvere, U., Kolberg, L., Kuzmin, I., Arak, T., Adler, P., Peterson, H., and Vilo, J. (2019). g:Profiler: a web server for functional enrichment analysis and conversions of gene lists (2019 update). Nucleic Acids Res *47*, W191-W198.
Resh, M.D. (2006). Palmitoylation of ligands, receptors, and intracellular signaling molecules. Science's STKE : signal transduction knowledge environment *2006*, re14.
Rieder, C.L., and Khodjakov, A. (2003). Mitosis through the microscope: advances in seeing inside live dividing cells. Science *300*, 91-96.
Rosenblatt, J. (2008). Mitosis: moesin and the importance of being round. Curr Biol *18*, R292-293.
Roux, K.J., Kim, D.I., Raida, M., and Burke, B. (2012). A promiscuous biotin ligase fusion protein identifies proximal and interacting proteins in mammalian cells. J Cell Biol *196*, 801-810.
Shalem, O., Sanjana, N.E., Hartenian, E., Shi, X., Scott, D.A., Mikkelson, T., Heckl, D., Ebert, B.L., Root, D.E., Doench, J.G., *et al.* (2014). Genome-scale CRISPR-Cas9 knockout screening in human cells. Science *343*, 84-87.
Stewart, M.P., Helenius, J., Toyoda, Y., Ramanathan, S.P., Muller, D.J., and Hyman, A.A. (2011a). Hydrostatic pressure and the actomyosin cortex drive mitotic cell rounding. Nature *469*, 226-230.
Stewart, M.P., Toyoda, Y., Hyman, A.A., and Muller, D.J. (2011b). Force probing cell shape changes to molecular resolution. Trends Biochem Sci *36*, 444-450.

bioRxiv preprint doi: https://doi.org/10.1101/2020.05.24.111831; this version posted May 24, 2020. The copyright holder for this preprint (which was not certified by peer review) is the author/funder, who has granted bioRxiv a license to display the preprint in perpetuity. It is made available under aCC-BY-NC-ND 4.0 International license.

Straight, A.F., Cheung, A., Limouze, J., Chen, I., Westwood, N.J., Sellers, J.R., and Mitchison, T.J. (2003). Dissecting temporal and spatial control of cytokinesis with a myosin II Inhibitor. Science *299*, 1743-1747.
Stypulkowski, E., Asangani, I.A., and Witze, E.S. (2018). The depalmitoylase APT1 directs the asymmetric partitioning of Notch and Wnt signaling during cell division. Sci Signal *11*.
Szklarczyk, D., Gable, A.L., Lyon, D., Junge, A., Wyder, S., Huerta-Cepas, J., Simonovic, M., Doncheva, N.T., Morris, J.H., Bork, P., *et al.* (2019). STRING v11: protein-protein association networks with increased coverage, supporting functional discovery in genome-wide experimental datasets. Nucleic Acids Res *47*, D607-D613.
Taguchi, Y., Mistica, A.M., Kitamoto, T., and Schatzl, H.M. (2013). Critical significance of the region between Helix 1 and 2 for efficient dominant-negative inhibition by conversion-incompetent prion protein. PLoS Pathog *9*, e1003466.
Tai, K., Kubota, M., Shiono, K., Tokutsu, H., and Suzuki, S.T. (2010). Adhesion properties and retinofugal expression of chicken protocadherin-19. Brain Res *1344*, 13-24.
Uretmen Kagiali, Z.C., Saner, N., Akdag, M., Sanal, E., Degirmenci, B.S., Mollaoglu, G., and Ozlu, N. (2020). CLIC4 and CLIC1 bridge plasma membrane and cortical actin network for a successful cytokinesis. Life Sci Alliance *3*.
Uyeda, T.Q., Kitayama, C., and Yumura, S. (2000). Myosin II-independent cytokinesis in Dictyostelium: its mechanism and implications. Cell Struct Funct *25*, 1-10.
Webb, Y., Hermida-Matsumoto, L., and Resh, M.D. (2000). Inhibition of protein palmitoylation, raft localization, and T cell signaling by 2-bromopalmitate and polyunsaturated fatty acids. J Biol Chem *275*, 261-270.
Zhou, X., Updegraff, B.L., Guo, Y., Peyton, M., Girard, L., Larsen, J.E., Xie, X.J., Zhou, Y., Hwang, T.H., Xie, Y., *et al.* (2017). PROTOCADHERIN 7 Acts through SET and PP2A to Potentiate MAPK Signaling by EGFR and KRAS during Lung Tumorigenesis. Cancer Res *77*, 187-197.